MDPI

Review

Prenucleation at the Liquid/Substrate Interface: An Overview

Hua Men, Changming Fang and Zhongyun Fan *

Brunel Centre for Advanced Solidification Technology (BCAST), Brunel University London,
Uxbridge UB8 3PH, Middlesex, UK
* Correspondence: zhongyun.fan@brunel.ac.uk; Tel.: +44-1895-266406

Abstract: Prenucleation refers to the phenomenon of substrate-induced atomic ordering in the liquid adjacent to the liquid/substrate interface at temperatures above the nucleation temperature. We investigated the effects of the physical and chemical properties of the substrate on prenucleation, using the classical molecular dynamics (MD) and ab initio MD simulations. We found that the physical origin of prenucleation is structural templating, which is affected significantly by the lattice misfit between the solid and the substrate, chemical interaction between the solid and the substrate, and the substrate surface roughness at the atomic level. Prenucleation ultimately determines the nucleation potency of a substrate and provides a precursor for heterogeneous nucleation at the nucleation temperature. In this paper, we provide an overview of the recent advances in the understanding of prenucleation made by the LiME Research Hub. After a brief review of the historical research on atomic ordering at the liquid/substrate interface in the literature, we present an overview of the recent advances in understanding prenucleation, covering the concept of prenucleation, the effect of temperature, lattice misfit and substrate chemistry, and substrate surface roughness at the atomic level. Our discussions will be focused on the effect of prenucleation on heterogeneous nucleation and its consequences on grain refinement.

Keywords: interface; nucleation; MD simulation; atomic ordering; lattice misfit; dislocations

1. Introduction

The nucleation of crystals in liquids is one of the most ubiquitous phenomena in both natural and industrial processes [1,2]. Understanding nucleation is therefore of importance to both science and technology, such as ice nucleation for climate control [3,4], the solidification and casting of metallic materials [5], the manipulation of nucleation of molecular crystals in the context of drug design and production [6], and protein crystal formation in living beings [7].

Our current understanding of nucleation is far from complete, and nucleation research has been dominated by the classical nucleation theory (CNT) for more than a century [1,2]. In the heterogeneous CNT, a spherical cap of the solid phase with a critical size forms on a substrate through fluctuations of atomic configuration, chemical composition, and temperature in the undercooled liquid [1]. The liquid adjacent to the substrate is assumed to be completely disordered prior to heterogeneous nucleation. However, theoretically, there is a massive gap of 10^{10} $m^{-3}s^{-1}$ in the homogeneous ice nucleation rate between computer simulations and experimental measurements, which has triggered an intense debate between theoreticians and experimentalists in the past decade [4]. In practice, the CNT provides little guidance on nucleation control in important industrial processes. For example, although the TiB_2-based grain refiner has been used in the metallurgical industry for over 80 years [8], it was mainly developed by trial-and-error, with little help from the CNT.

Recent theoretical and experimental findings suggest that the atoms in the liquid at the liquid/substrate interface become layered within a few atomic layers away from the interface (atomic layering), and the atoms within the individual layers may have a

significantly ordered structure (in-plane atomic ordering) even at temperatures above the liquidus [9]. It has been speculated that such atomic ordering may have significant influence on the subsequent heterogeneous nucleation process [10]. On the other hand, the epitaxial nucleation model [11] proposes a structural templating mechanism for heterogeneous nucleation. The substrate lattice provides a template for the formation of the new phase, and the dislocations at the interface accommodate the lattice misfit between the new phase and the substrate. Such substrate-induced atomic ordering can be attributed to structural templating. Both experimental observations [12,13] and atomistic simulations [14–17] have provided direct evidence to support the structural templating mechanism.

Atoms in the liquid at the interface may have a structure different from either the bulk liquid (short-range order) or crystalline solid (long-range order), with an atomic ordering being in between the bulk liquid and the bulk solid. Recently, we developed the concept of prenucleation to better describe the substrate-induced atomic ordering in the liquid at the interface, which persists until the occurrence of heterogeneous nucleation at a certain undercooling [18]. The terminology of the prenucleation is firstly used by the chemistry research community to describe the stable atomic clusters (usually denser liquid) formed in a solution, inside which homogeneous nucleation occurs [19]. We extend the concept of prenucleation to a wider and more general case of heterogeneous nucleation, since homogeneous nucleation is rare in reality. It is reported that the degree of atomic ordering in the liquid at the interface is closely related to the nature of the substrate, such as crystal structure and surface orientation [14]. To date, there is still a dearth of systematic investigation into the effects of the physical and chemical properties of the substrate on both prenucleation and the subsequent heterogeneous nucleation. For example, the most relevant physical property to heterogeneous nucleation is the lattice misfit (f) between the new solid phase and the substrate. The crystallographic model of Turnbull and Vonnegut [20] suggests that the potency of the substrate is inversely proportional to misfit. On the other hand, the epitaxial model indicates that nucleation potency degrades with increasing misfit up to a limit of 12.5% [11]. Experimental observations [21,22] showed that nucleation undercooling, ΔT_n, increases initially with increasing misfit, and reaches a peak around $f = 13\%$, and then decreases with a further increase in misfit. The magnitude of ΔT_n is a good indicator of the potency of the substrate for a given liquid. It seems that the potency of the substrate is not a monotonic function of misfit [23], and cannot be interpreted adequately in terms of the mechanism of the heterogeneous nucleation described by Turnbull's model.

The atomic structure of the liquid/substrate interface can be changed substantially by prenucleation, which in turn will produce a significant impact on the subsequent heterogeneous nucleation process. Fan and co-workers have intensively investigated the effects of the physical and chemical properties of the substrate, such as lattice misfit, substrate chemistry, and surface roughness, on prenucleation in the past decade [18,24–27].

In this paper, we provide an overview of the recent advances in the understanding of prenucleation made by the LiME Research Hub. After a brief review of the historical research on atomic ordering at the liquid/substrate interface in Section 2, we present an overview of the recent advances in prenucleation made by the Hub in Section 3, covering the concept of prenucleation, the effect of temperature, lattice misfit and substrate chemistry, and substrate surface roughness. Our discussions in Section 4 focus on the effect of prenucleation on heterogeneous nucleation and its consequences on grain refinement.

2. Historical Development

2.1. The "Hard Wall" Effect

The atomic layering in the liquid at the liquid/substrate interface was attributed to the "hard wall" effect. Henderson et al. [28] obtained the density profile of a hard-sphere fluid in contact with a structureless hard wall by solving the Ornstein–Zernike equation in the Percus–Yevick approximation. It was demonstrated that the liquid near the wall was layered with a density that decays with the distance, z, from the wall. Abraham

and Singh [29,30] confirmed this conclusion by treating the structureless wall as a soft repulsive/attractive structureless wall, using analytical methods and Monte Carlo (MC) simulations. This phenomenon, that the liquid has an oscillatory density profile at the interface with a solid wall, was referred to as the "hard wall" effect [31,32].

2.2. Atomistic Simulations

Atomistic simulations offer direct access to microscopic details of the liquid/solid interface, and here, research interest has been focused on the liquid/substrate interface. Rull and Toxvaerd [33] studied the atomic ordering of a Lennard–Jones (LJ) liquid adjacent to static fcc (100), fcc (111), and bcc (100) surfaces using MD simulations. It was observed that the density oscillations (layering) decay exponentially with the distance from the interface, approximately according to $\exp(-z/\xi\Delta z^2)$, where Δz is the mean interlayer spacing and ξ is the correlation length for the interface region. The degree of in-plane atomic ordering was mainly determined by the repulsive part of the interaction. Kyrlidis and Brown [34] performed MC simulations for the (111), (110), and (100) interfaces. They revealed that the number of the layering was 4–5, 5–6, and 4 for the (100), (111), and (110) interfaces, respectively, and the interfacial layer spacing was larger for the (100) interface than that for the (111) interface.

Using the MD simulation with adapted *n*-body potentials, Geyermans et al. [35] reported that a solid Cu wall induced significant layering in the interfacial liquid Al, largely independent of the surface orientation of the substrates. Employing a semi-empirical potential of an embedded-atom method (EAM), Hashibon et al. [14,15] confirmed an exponential decay of the atomic density profile in the liquid Al at the interface, and found that there was far greater in-plane ordering in the liquid in contact with a bcc (100) substrate than that with a bcc (110) substrate. Furthermore, Palafox-Hernandez et al. [16] observed 2 to 3 "prefreezing" interfacial layers in liquid Pb in contact with solid Cu (111) planes, but no such prenucleation was found with solid Cu (100) planes.

Using ab initio MD simulations, Wang et al. [17] observed an fcc-like ordering in the liquid Al in contact with Ti-terminated TiB_2, but not with B-terminated TiB_2. It revealed that the growth of the α-Al was frustrated by the lattice misfit between the solid Al and TiB_2 substrate at a relatively small undercooling.

All of these studies suggest that the atomic ordering at the interface is distinct from that of bulk liquid, and is highly dependent on the structure and chemistry of the substrate for a given liquid.

2.3. Experimental Observations

Surface-induced atomic layering in liquid Ga and Hg has been observed using X-ray reflectivity [36–38], indicating that the layering solely results from the "hard wall" effect.

It is not a trivial task to access the atomic structure at the liquid/substrate interface with the experimental observations, since the interface is buried inside the condensed phases. Experimental observations confirmed that substrates could induce atomic ordering in the liquid at the interface [29,39–42]. Using the X-ray diffuse scattering method, Grey et al. [43] revealed that liquid Pb on (111) Ge substrates exhibited a ring of diffuse scattering with a radial spatial frequency, significantly different from that in bulk liquid Pb. With specular X-ray reflectivity, Huisman et al. [39,44] and Huisman and van der Veen [45] observed pronounced layering of the liquid Ga in contact with a (111) diamond surface, which decayed exponentially with increasing distance from the interface. The atoms in the liquid Ga near the substrate surface may assume a solid-like structure similar to that of α-Ga. Reedijk et al. [46] found that the liquid Sn exhibited layering and in-plane atomic ordering at the interface with (111) Ge substrate, where Sn atoms changed gradually from solid-like to more liquid-like with increasing temperature. In another study [47], the authors reported that KDP (KH2PO4) crystal induced ordering in the first four interfacial layers of H_2O molecules, where the first two layers exhibited ice-like behaviour and the next two layers showed only minor lateral and perpendicular ordering.

Through HRTEM (high-resolution transmission electron microscopy) observation, Oh et al. [12,13] provided direct evidence for the atomic layering and in-plane ordering in liquid Al in contact with an α-Al$_2$O$_3$ substrate. It revealed that the Al atoms at the interface had a high degree of structural correlation to the crystal structure of the α-Al$_2$O$_3$ substrate. On the other hand, using in situ X-ray scattering, Schülli et al. [48] found that the Au atoms in AuSi eutectic droplets had a pentagonal atomic arrangement in contact with a Si (111) substrate. They proposed that this pentagonal atomic arrangement in the liquid at the interface caused a lateral-ordering stabilisation process, which was the main barrier for heterogeneous nucleation.

All of these studies confirmed that the atoms in the liquid became layered within a few atomic layers away from the surface or interface, due to the "hard wall" effect [49,50], and it was consistent with the theoretical calculations [29,51–54]. There also may exist pronounced in-plane atomic ordering at the interface, which is highly relevant to the lattice structure of the substrate.

3. Recent Advances

Under the LiME Hub (www.lime.ac.uk, accessed on 5 September 2022) research programme, we have systematically investigated atomic ordering in the liquid adjacent to a liquid/substrate interface. For this purpose, a generic simulation system was created to make the simulation results more generally applicable [18,24,25]. This simulation system consists of a generic liquid and a generic fcc substrate with a <111> surface orientation, where the z axis is normal to the {111} plane of the substrate. We chose Al as the generic liquid since it represents many metals in terms of liquid atomic structures. The generic fcc substrate was built by pinning Al atoms with a specified lattice parameter to pre-set the lattice misfit [25]. There are two major advantages to this generic system. Firstly, it allows us to simulate nucleation systems with substrates of high melting temperatures (T_1), which are similar to the nuclean particles used in industrial practices (e.g., TiB$_2$ with T_1 = 3498 K). Secondly, this makes it possible for simulating the effect of lattice misfit alone without interference from the chemical interaction between the liquid and substrate and/or the substrate surface roughness at atomic level [26,27]. For simplicity, we have used the generic terms "the liquid" and "the substrate". In this section, we introduce the concept of prenucleation and examine the effects on prenucleation of temperature, lattice misfit, substrate surface roughness, and chemical interaction between the liquid and the substrate.

3.1. Concept of Prenucleation

Prenucleation refers to the phenomenon of atomic ordering in the liquid adjacent to the liquid/substrate interface at temperatures above the nucleation temperature. It can be described in three distinctive ways depending on the purpose of the study. From the viewpoint of atomic arrangement at the interface, prenucleation can be quantified by atomic layering and in-plane atomic ordering; for considering structural formation, prenucleation is better described as the formation of a two-dimensional (2D) ordered structure at the interface; and for atomistic understanding of interfacial energy, prenucleation can be considered as the formation of a diffuse liquid/substrate interface. In this section, the concept of prenucleation is introduced and analysed in these three ways.

3.1.1. Layering and In-Plane Atomic Ordering

Figure 1a gives an example of snapshots of the generic liquid/substrate system with -2% misfit at T = 900 K, showing a layered structure in the liquid at the interface. The corresponding atomic density profile shows that there are six atomic layers with decreasing peak density away from the interface (Figure 1b), while only the first three atomic layers contain some degree of in-plane atomic ordering (Figure 1c). Consequently, the first layer (L1) exhibits a nearly ordered structure (Figure 1d), the second layer (L2) shows a mixed structure of ordered and disordered regions (Figure 1e), and the third layer (L3) is largely disordered (Figure 1f).

Atomic layering can be quantified by the atomic density profile, $\rho(z)$, for the ordering normal to the interface [14]:

$$\rho(z) = \frac{\langle N_z \rangle}{L_x L_y \Delta z},$$

(1)

where N_z is the number of atoms between $z - \Delta z/2$ and $z + \Delta z/2$ at time t, and Δz is the width of the bin. The angled brackets indicate a time-averaged quantity, and L_x and L_y are the x and y dimensions of the bin, respectively. As an example, Figure 1b shows the $\rho(z)$ as a function of distance from the interface for the same simulation system equilibrated at 900 K. The atomic layering persists within six atomic layers at the interface. The peak density decreases sharply from 0.31 atom/Å^3 for L1 to 0.05 atom/Å^3 beyond the sixth layer, which is the average atomic number density of the bulk liquid.

The in-plane atomic ordering can be characterised by the in-plane order parameter, $S(z)$, for the ordering parallel to the interface [55]:

$$S(z) = \frac{\left| \sum_{j \in \Delta z} exp\left(i\boldsymbol{K} \cdot \boldsymbol{r}_j \right) \right|^2}{N_z^2},$$

(2)

where the summation is over all atoms labelled j within a given bin of width, Δz, of one layer spacing and $\boldsymbol{K}$ is a reciprocal lattice vector, and $\boldsymbol{r}_j$ is the position vector of the jth atom in the Cartesian space. The in-plane atomic ordering decreases sharply from L1 to L3 and diminishes beyond L3 for the same system (Figure 1c). This indicates that in-plane atomic ordering decays faster than the atomic layering away from the interface, implying that atomic layering and in-plane ordering are governed by different atomistic mechanisms; as will be discussed later, this includes the "hard wall" effect for the atomic layering and structural templating for the in-plane atomic ordering.

3.1.2. Two-Dimensional Ordered Structure

The 2D ordered structure at the liquid/substrate interface is a direct outcome of prenucleation. There exists the solid-like structure at the interface, although it is not the new (bulk) phase. The 2D ordered structure can be identified by employing the local bond-order analysis [56], which is an approach widely used in atomistic simulations to distinguish solid atoms from liquid atoms [57–59]. To perform the local bond-order analysis, the local bond-order parameter, $\boldsymbol{q}_l(i)$, is calculated by [56]:

$$\boldsymbol{q}_l(i) = \left(\frac{4\pi}{2l+1} \sum_{m=-l}^{l} |\boldsymbol{q}_{lm}(i)|^2 \right)^{\frac{1}{2}}$$

(3)

where the $(2l + 1)$ dimensional complex vector $\boldsymbol{q}_{lm}(i)$ is the sum of spherical harmonics, $Y_{lm}(\boldsymbol{r}_{ij})$, over all of the nearest neighbouring atoms of the atom i. Two neighbouring atoms, i and j, can be recognised to be connected if the correlation function, $\boldsymbol{q}_6(i) \cdot \boldsymbol{q}_6(j)$, of the vector $\boldsymbol{q}_6$ of neighbouring atoms i and j exceeds a certain threshold. An atom is identified as being in the solid state if the number of connections of this atom with its neighbours is larger than a threshold. A 2D ordered structure is shown in Figure 2a for the system with −2% misfit equilibrated at 900 K after the liquid-like atoms are removed from the snapshot. The 2D ordered structure extends up to L3, but may not cover the entire substrate surface.

3.1.3. Diffuse Liquid/Substrate Interface

One of the important consequences is that the liquid/substrate interface is not sharp, but diffuse within a few atomic layers (Figure 2b). The atoms in the liquid at the interface have a layered structure within a few atomic layers, and the in-plane atomic ordering may exist in the first few atomic layers. Such diffuse interfaces may have profound effects on many scientifically and technologically important processes occurring at the liquid/substrate interface, such as heterogeneous nucleation, catalysis, wetting, chemical segregation, crystal growth, lubrication, and liquid-phase epitaxy.
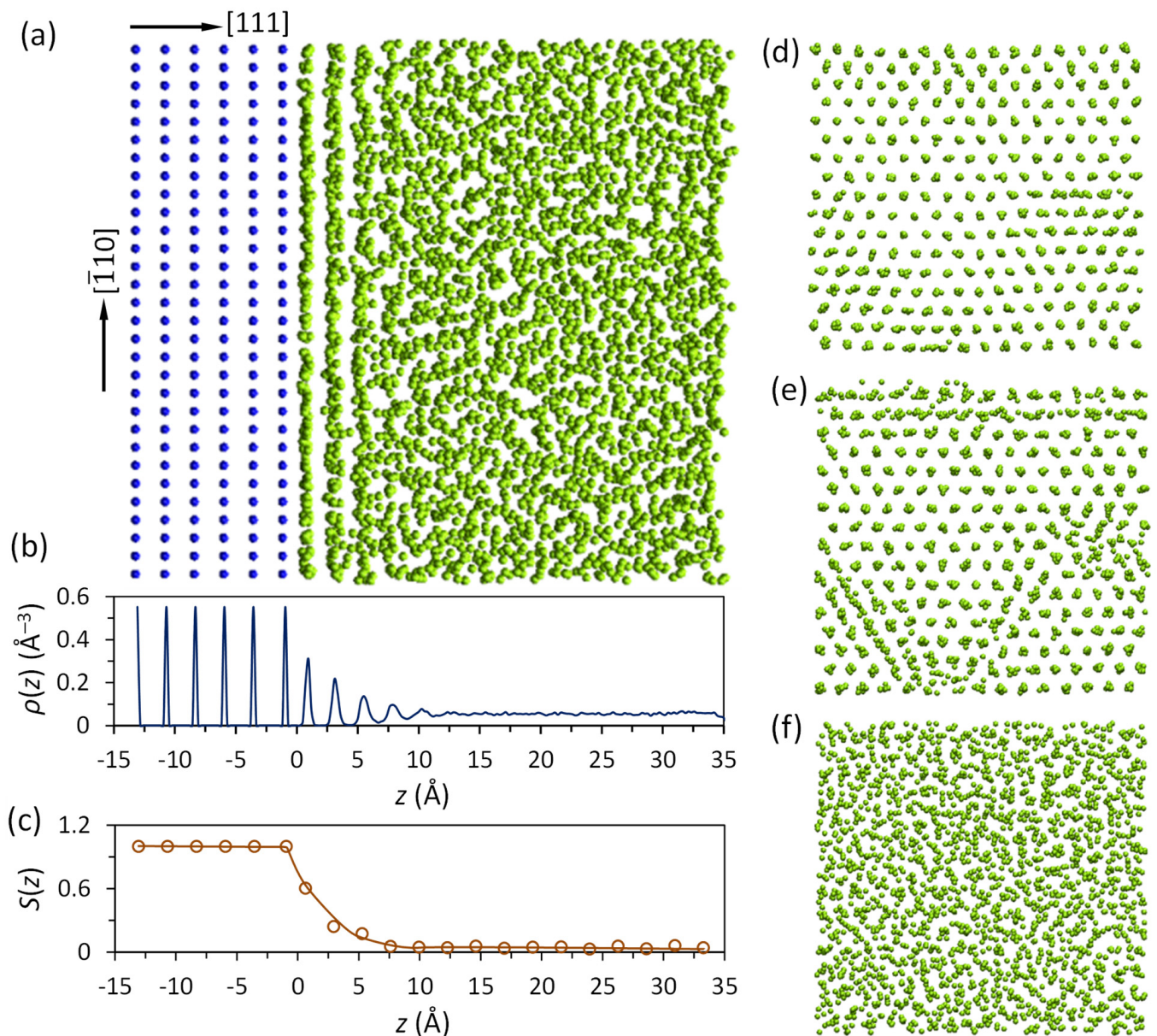
Figure 1. Prenucleation manifested by atomic layering and in-plane atomic ordering at the liquid/substrate interface [18]. A generic liquid/substrate system with −2% misfit has been equilibrated at 900 K for 1 ns. (**a**) A snapshot showing the time-averaged atomic positions in the system; (**b**) the quantified atomic density profile, $\rho(z)$, and (**c**) in-plane order parameter, $S(z)$, as a function of distance (z) away from the interface for the system showing that atomic layering in the liquid persists within six atomic layers at the interface, with significant in-plane atomic ordering within the first two atomic layers. The time-averaged atomic positions in (**d**) the first layer (L1), (**e**) the second layer (L2), and (**f**) the third layer (L3) suggest that L1 and L2 exhibit a mixed structure of ordered and disordered regions, and L3 has a largely disordered structure. The blue and green spheres represent atoms in the substrate and liquid, respectively. (Reprinted with permission from Ref. [18]. Copyright 2022, Spring Nature).
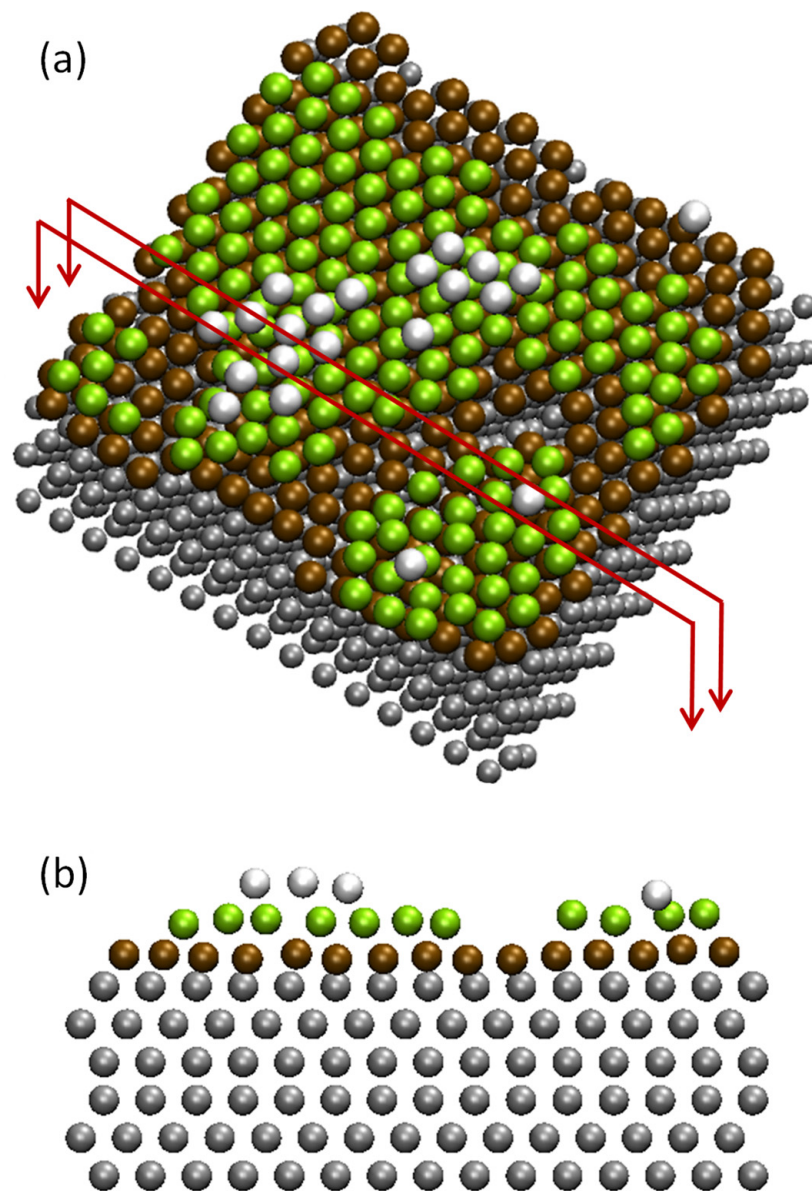
Figure 2. Two-dimensional (2D) ordered structure and diffuse liquid/substrate interface. (**a**) A snapshot of the simulation system with −2% misfit equilibrated at 900 K showing the 2D ordered structure formed on the surface of the substrate; and (**b**) front view of a slab, taken from the position marked in (**a**), showing the ordered atoms in a diffuse interface between the liquid and the substrate. The results were obtained by local bond-order analysis. The light spheres represent the solid-like atoms in the interfacial layers (ochre, green, and white online for L1, L2, and L3, respectively), and the dark (grey online) spheres represent the substrate atoms.

3.2. Effect of Temperature

We investigated the evolution of the atomic ordering in the liquid at the liquid/substrate interface as a function of temperature. Atomic layering is only slightly enhanced with decreasing temperature from 1400 K to 900 K for the generic liquid/substrate system with −2% misfit, in terms of the number of atomic layers and the corresponding peak density for the layered structure at the interface (Figure 3a). The layering persists within four atomic layers at 1400 K, and increases to six atomic layers at 900 K. In contrast, the in-plane atomic ordering diminishes at high temperatures, with an $S(z)$ of 0.07 for L1 at 1400 K, which is close to 0.05 of the bulk liquid (Figure 3b). The in-plane atomic ordering is enhanced significantly with decreasing temperature, and the $S(z)$ of L1 increases dramatically to 0.61 at 900 K.

This suggests that, in general, prenucleation is a continuous transition from the liquid-like structure (only with short-range order) to the solid-like structure (with long-range order in 2D) while the temperature is lowered. This trend will continue for the temperatures below the liquidus until the occurrence of heterogeneous nucleation under a certain undercooling.
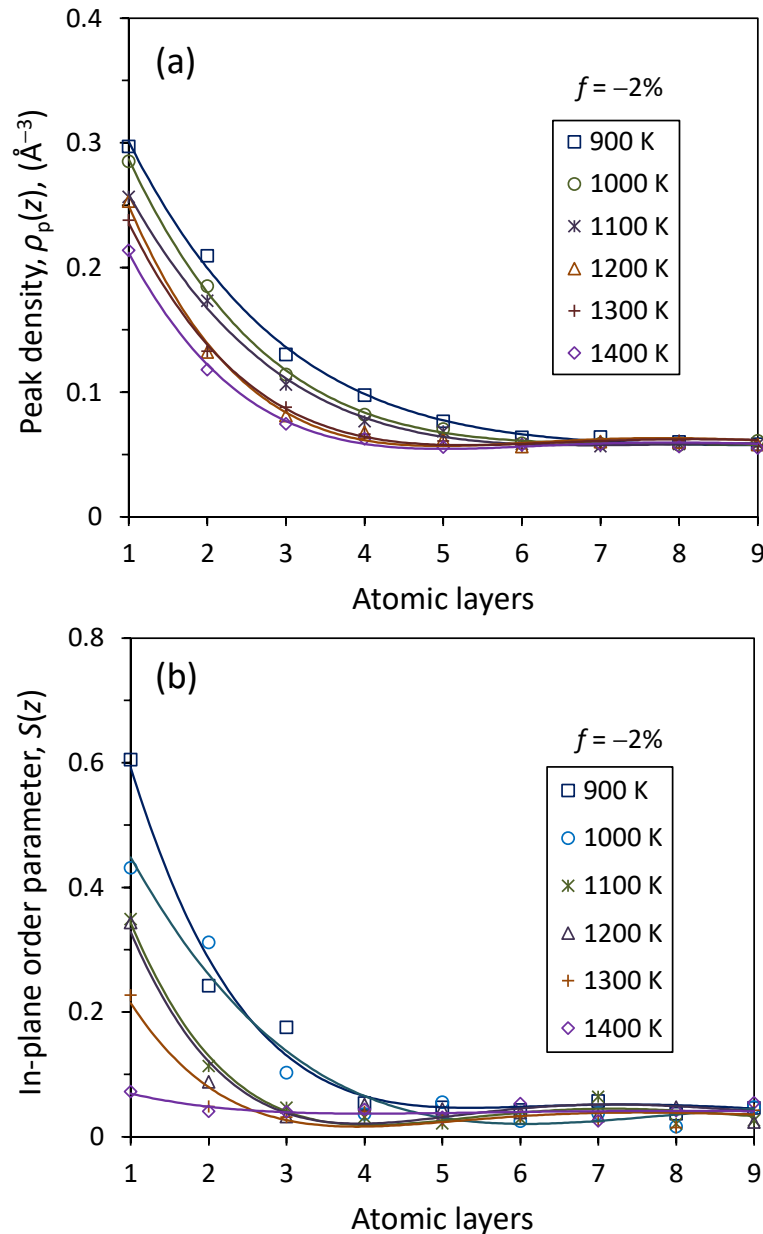
Figure 3. Temperature effect on prenucleation [18]. (**a**) Peak density, $\rho_P(z)$, of the density profile and (**b**) in-plane atomic order parameter, $S(z)$, as functions of temperature, T, and atomic layers away from the interface for the system with -2% misfit. The scattered data and solid lines represent the calculated values of $\rho_P(z)$ or $S(z)$ and the fitted lines, respectively. Both the atomic layering and in-plane atomic ordering decrease with increasing T. However, at $T = 1400$ K, the in-plane atomic ordering almost vanishes, while the atomic layering persists within approximately four atomic layers. (Reprinted with permission from Ref. [18]. Copyright 2022, Spring Nature.)

3.3. Effect of Lattice Misfit

Lattice misfit (f) is defined as $f = (d_S - d_N)/d_S$, where d_S and d_N are the atomic spacing of the solid and the substrate, respectively [11]. The epitaxial nucleation model [11] suggests that the potency of a substrate for heterogeneous nucleation decreases with increasing

lattice misfit when $|f| < 12.5\%$. Thus, prenucleation would have a significant effect on the nucleation potency of the substrate. Further, the epitaxial nucleation model [11] predicts that the theoretical limit of the lattice misfit that the dislocations mechanism can accommodate is 12.5%. Here, we divide nucleation systems into two categories: systems with small misfit ($|f| < 12.5\%$) and systems with large misfit ($|f| > 12.5\%$). In this section, we present the atomic configurations at the liquid/substrate interface in the systems with different misfits.

3.3.1. Prenucleation on Substrates with Small Negative Misfit ($-12.5\% < f < 0$)

To examine the effect of the small lattice misfit ($|f| < 12.5\%$), the classical MD simulations were conducted with the DL_POLY_4.08 MD package for the generic liquid/substrate systems [18,24], which has a misfit less than 12.5%, either negative or positive, with the solid α-Al. The EAM potential for Al, developed by Zope and Mishin to model interatomic interactions [60], was used.

Atomic layering is independent of misfit, and in-plane atomic ordering is significantly enhanced by reducing the value of misfit for small negative misfit. We investigated the atomic ordering in the liquid Al at the interface with pinned substrates for the lattice misfits in a range of 0% to -10%. The atomic layering persists within six layers from the interface for the systems with varied misfit equilibrated at 1000 K. The $\rho_{\rm p}$ and interlayer spacing, $d_{\rm a}$, exhibit negligible variation with misfit (Figure 4a,c), suggesting that the layering is largely independent of misfit. On the other hand, the in-plane atomic ordering ($S(z)$) is strongly dependent on misfit. The liquid atoms at the interface exhibit pronounced in-plane atomic ordering within the first three atomic layers when misfit is small, but the in-plane ordering becomes weak when misfit is large (Figure 4b).

A 2D ordered structure exists at the interface for all of the systems with small negative misfit, as evidenced by the atomic arrangements in L1 superimposed on the surface layer of the substrate (L0) with varied misfit equilibrated at 900 K (Figure 5). For 0% misfit, L1 consists of solid-like atoms, which are epitaxial to the substrate lattice (Figure 5a). With increasing misfit, L1 changes into a mixed structure of ordered and disordered regions, which consist of the solid-like and liquid-like atoms (Figure 5b–d). The atoms in the ordered regions in L1 are epitaxial to the lattice of the substrate. This suggests that the formation of the 2D ordered structure in the liquid at the interface is achieved through structural templating.

3.3.2. Prenucleation on Substrates with Small Positive Misfit ($0\% < f < 12.5\%$)

Small positive lattice misfits produce effects on prenucleation very similar to those of small negative lattice misfits. The atomic layering is independent of the magnitude of the lattice misfit, and the in-plane atomic ordering deteriorates with increasing misfit [24]. However, a detailed examination of the atomic ordering at the liquid/substrate interface has revealed the difference in the two systems. In the systems with small positive misfit, L1 has a large constant in-plane atomic order parameter ($S(z) = 0.8$) for all of the systems, and it does not change with increasing misfit (Figure 6). $S(z)$ decreases sharply from L2 onwards with increasing misfit. Thus, the in-plane atomic ordering persists within about three atomic layers for $f = 0 - 2\%$, but reduces to two atomic layers for $f > 2\%$.

L1 is epitaxial to the surface layer of the substrate for all of the systems with small positive lattice misfits, as demonstrated by the time-averaged atomic positions of L1/L0, L2, and L3 for the system with 4% misfit at 1000 K (Figure 7). This is distinct from the systems with small negative lattice misfit. Here, L1 always has an ordered atomic arrangement, epitaxial to the L0 (Figure 7a). L2 has a mixed structure with ordered and disordered regions (Figure 7b), and L3 is almost disordered (Figure 7c). This suggests that there is a 2D ordered structure at the liquid/substrate interface for systems with small positive lattice misfit as well.
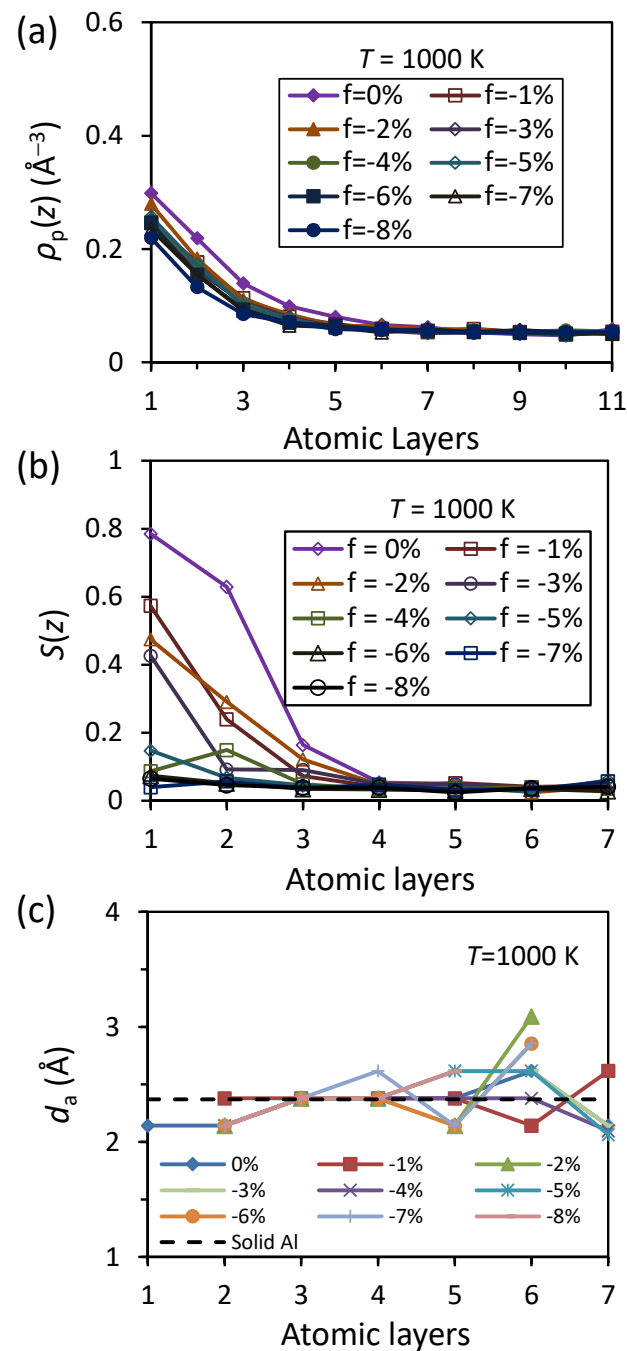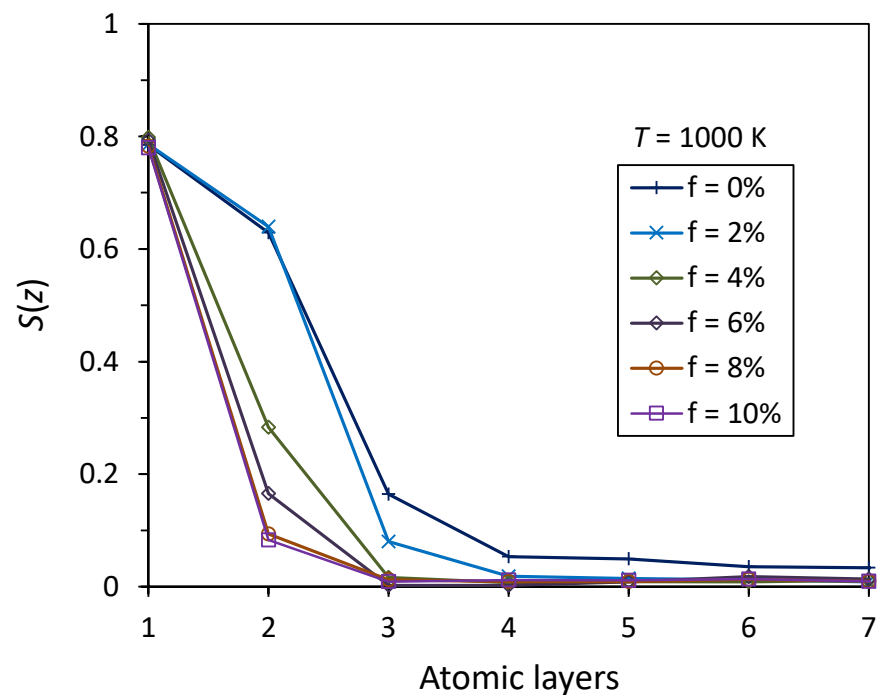
Figure 4. Prenucleation in systems with small negative misfits demonstrated by atomic layering and in-plane ordering [18]. (**a**) Peak density, $\rho_p(z)$, (**b**) in-plane atomic order parameter, $S(z)$, and (**c**) interlayer spacing, d_a, in the liquid at the interface are plotted as a function of atomic layers away from the interface for the systems with varied small negative misfit and equilibrated at 1000 K. Atomic layering and interlayer spacing are largely independent of misfit, while the in-plane ordering is strongly enhanced by reducing misfit. (Reprinted with permission from Ref. [18]. Copyright 2022, Spring Nature.)
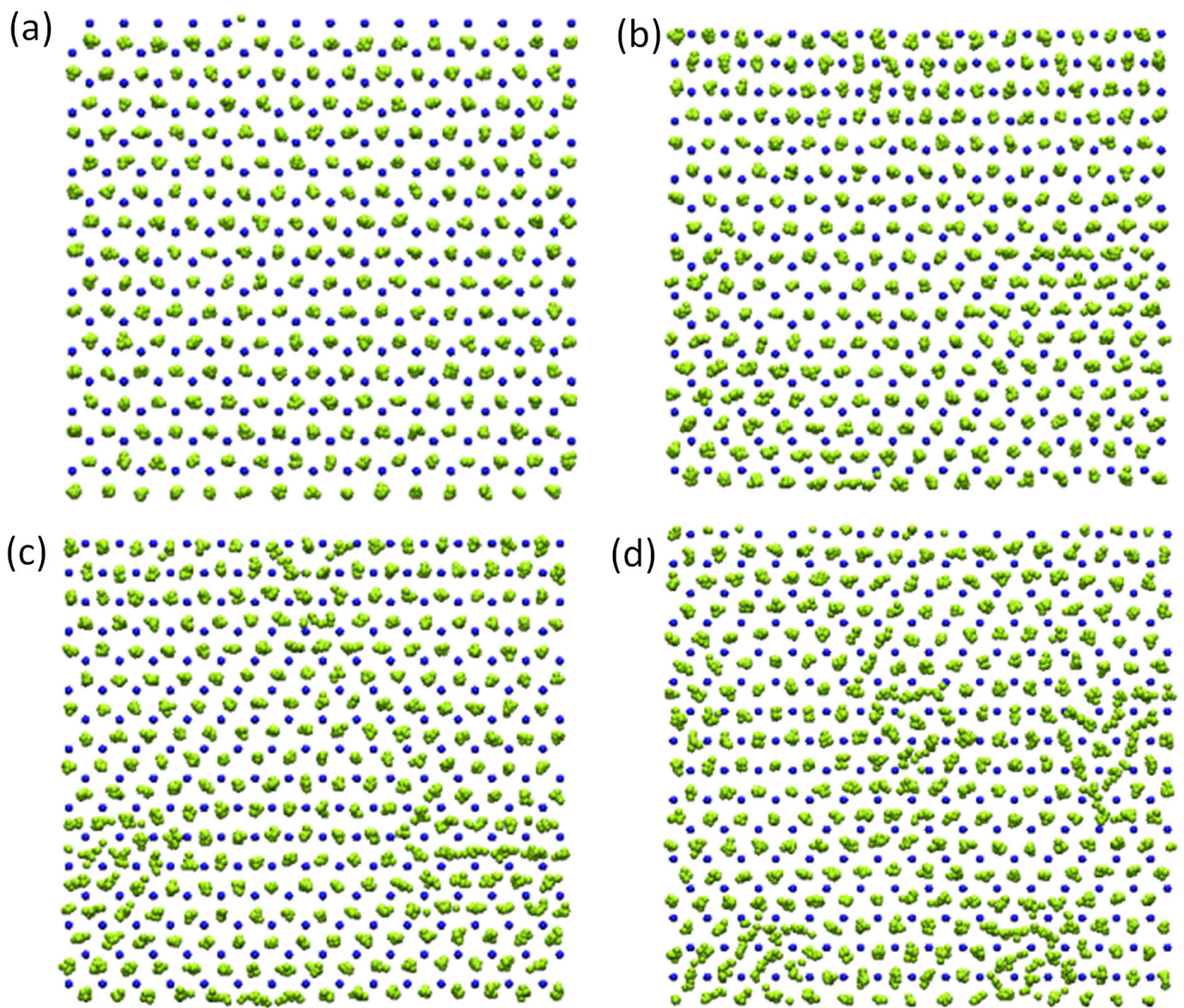
Figure 5. Prenucleation in systems with negative lattice misfits demonstrated by atomic ordering in L1 templated by the substrate [18]. Time-averaged atomic positions in L1 relative to the surface layer (L0) of the substrate, averaged over a period of 10 ps, are displayed for the systems with (**a**) $f = 0\%$, (**b**) -2%, (**c**) -4%, and (**d**) -8% equilibrated at 900 K. The blue and green spheres represent the atoms in the surface layer of the substrate and the first layer of the liquid (L1), respectively. For $f = 0\%$, L1 exhibits an almost fully ordered structure, which consists of the solid-like atoms. With increasing misfit, L1 becomes a mixed structure of ordered and disordered regions, with an increasing number of liquid-like atoms. The atoms in the ordered regions continue the lattice of the substrate. (Reprinted with permission from Ref. [18]. Copyright 2022, Spring Nature.)
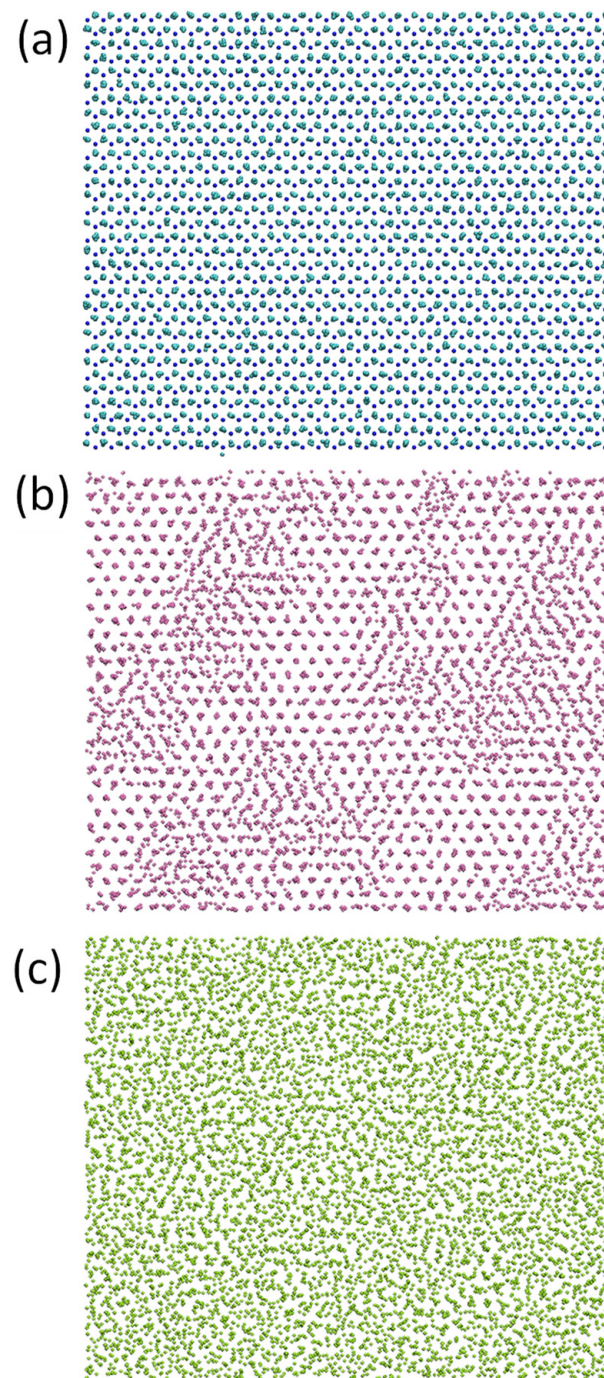
Figure 6. Prenucleation in systems with a small positive lattice misfit [24]. In-plane order parameter, *S*(*z*), as functions of lattice misfit and atomic layers away from the interface for the systems with small positive misfit, equilibrated at 1000 K. Generally, the in-plane atomic ordering degrades with increasing misfit. It is interesting to note that the *S*(*z*) of L1 is nearly the same (about 0.8) for all of the systems with varied misfit.

3.3.3. Prenucleation on Substrates with Large Misfit ($|f| > 12.5\%$)

For systems with a large lattice misfit, the liquid Pb/solid Cu (denoted as Pb(l)/Cu(s)) was used as an example [27], where the solid Pb and Cu have a large positive misfit of 27.3% along the close packed <110> directions on the close packed {111} planes. The EAM potentials for the Cu–Pb interatomic interactions, developed by Hoyt et al. [61], were implemented with the LAMMPS in the MD simulation [62].

We found that the atoms in the liquid at the interface exhibit pronounced atomic ordering even though the system has a large lattice misfit. On one hand, this confirms that, as a general trend, atomic layering at the interface is independent of lattice misfit. On the other hand, the pronounced in-plane atomic ordering at the interface with large lattice misfit does not follow the trend for small lattice misfit, either negative or positive. The time-averaged atomic positions of the first Cu(s) layer (L1Cu) and the first to the third Pb(l) layers (i.e., the CSL (coincidence site lattice)-Pb, L1Pb, L2Pb) in the Pb(l)/Cu(s) system equilibrated at 625 K are displayed in Figure 8a–d. The completely ordered Cu surface layer (L1Cu) (Figure 8a) templated two highly ordered layers in liquid Pb adjacent to the Pb(l)/Cu(s) interface, the CSL-Pb layer (Figure 8b) and L1Pb (Figure 8c). There are six transitional Pb(l) layers at the interface (Figure 8e), where the density profile is typical for the systems with an atomically flat substrate surface with either positive [24] or negative [18] lattice misfits. Only the first two liquid Pb layers adjacent to the interface have relatively high *S*(*z*) values (around 0.4), and further away from the interface, the *S*(*z*) value approaches zero (Figure 8f). This is indicative of the existence of a 2D ordered structure at the interface, consistent with the simulation results of Palafox-Hernandez et al. [16] who observed the 2–3 "prefreezing" layers of crystalline Pb at the liquid Pb/solid (111) Cu interface at 625 K.

Figure 7. Prenucleation in systems with small positive misfits [24]. The time-averaged atomic positions for (**a**) L1 on top of the surface layer of the substrate (L0), (**b**) L2, and (**c**) L3 in the liquid adjacent to the liquid/substrate interface with 4% misfit equilibrated at *T* = 1000 K. L1 has an ordered structure and is epitaxial to the L0, L2 has a mixed structure, and L3 is largely disordered.
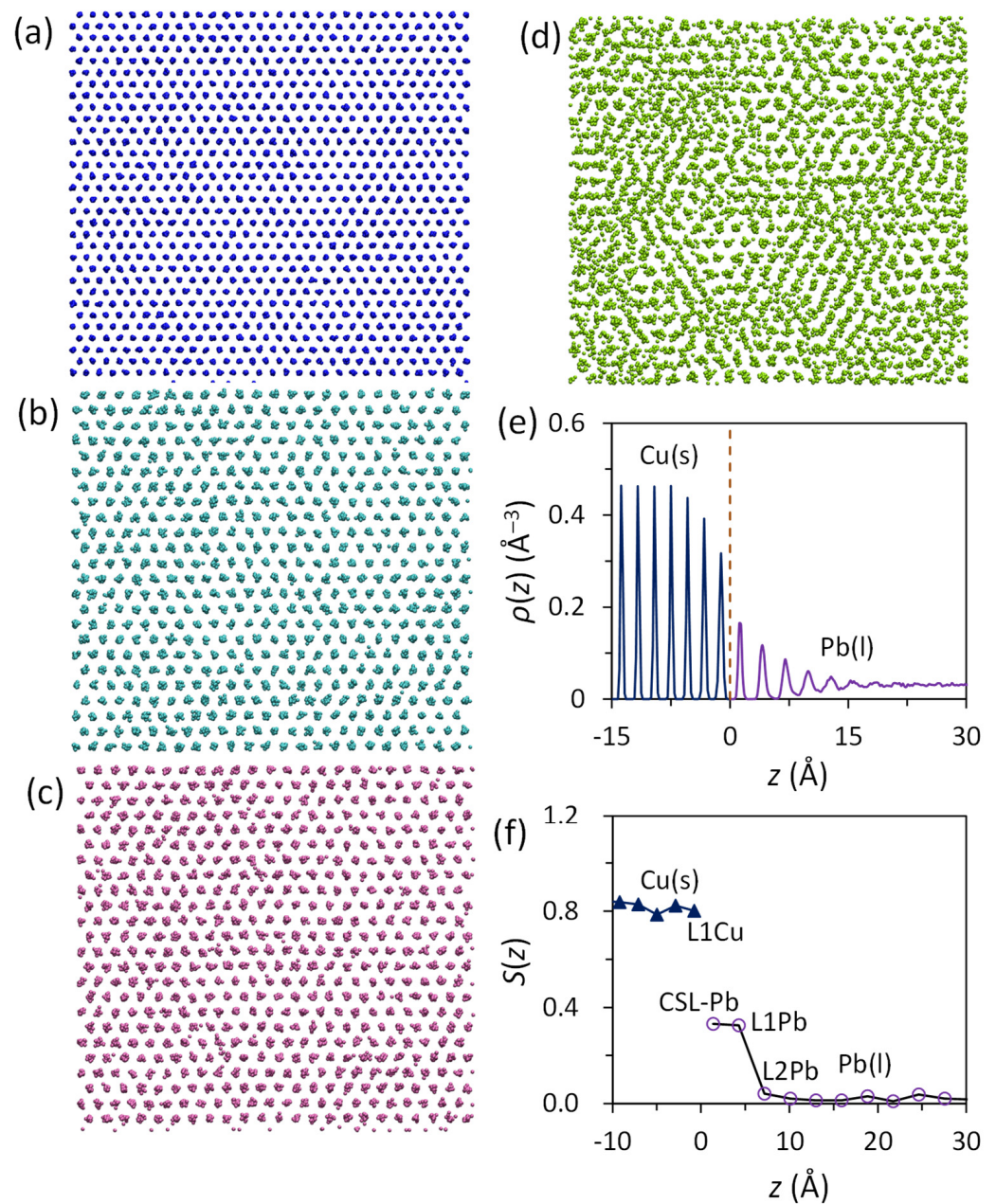
Figure 8. Prenucleation in systems with large positive misfit demonstrated by the Pb(l)/Cu(s) system [27]. Time-averaged atomic positions show the atomic arrangement of (**a**) the first Cu layer (L1Cu), (**b**) the CSL (coincidence site lattice) Pb layer; (**c**) first liquid Pb layer (L1Pb); and (**d**) the second liquid Pb layer (L2Pb) in the Pb(l)/Cu(s) system equilibrated at 625 K (above the melting temperature of Pb, 618 K). (**e**,**f**) show the $\rho(z)$ and $S(z)$ as a function of distance from the interface. There exists pronounced atomic ordering, including layering and in-plane atomic ordering, in the liquid Pb induced by the Cu substrate.

The quantified stress profile, $\sigma_s(z)$, as a function of distance from the interface for the Pb(l)/Cu(s) system equilibrated at 625 K is shown in Figure 9. It reveals the following facts: (1) the stress levels in the bulk liquid Pb and bulk solid Cu are close to zero, indicating that the Pb(l)/Cu(s) system at 625 K is in equilibrium; (2) the stress in the CSL-Pb layer is also close to zero; (3) the "*w*"-shaped stress profile suggests that the atoms in L1Pb, L1Cu, and L2Cu are in compression; and (4) the "*w*"-shaped stress profile is in good agreement with the result of Palafox-Hernandez et al. [16].
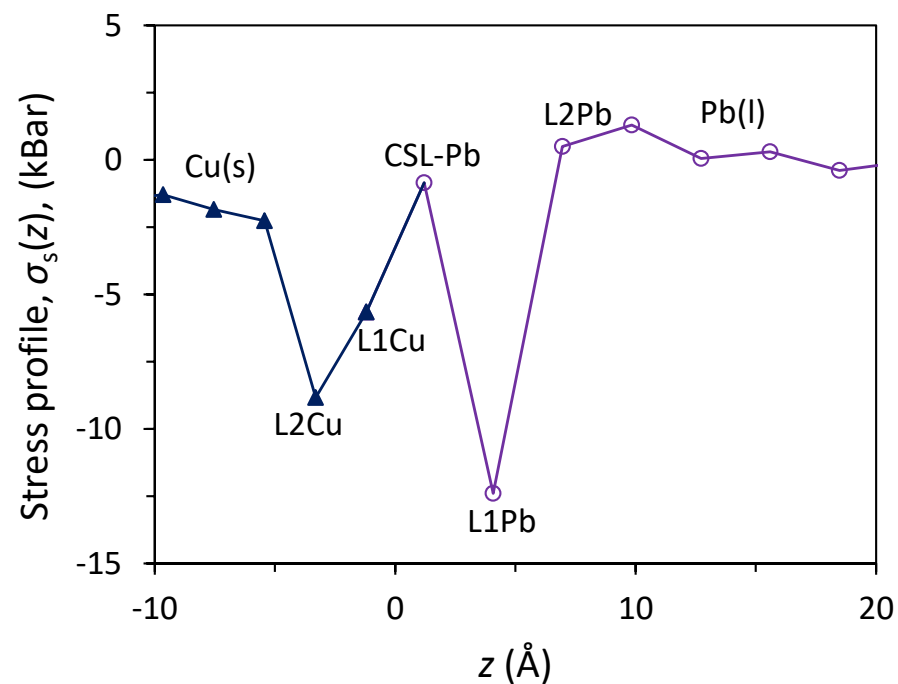
Figure 9. Stress state at the Pb(l)/Cu(s) interface [27]. Local stress distribution, $\sigma_s(z)$, as a function of distance away from the Pb(l)/Cu(s) interface, equilibrated at 625 K.
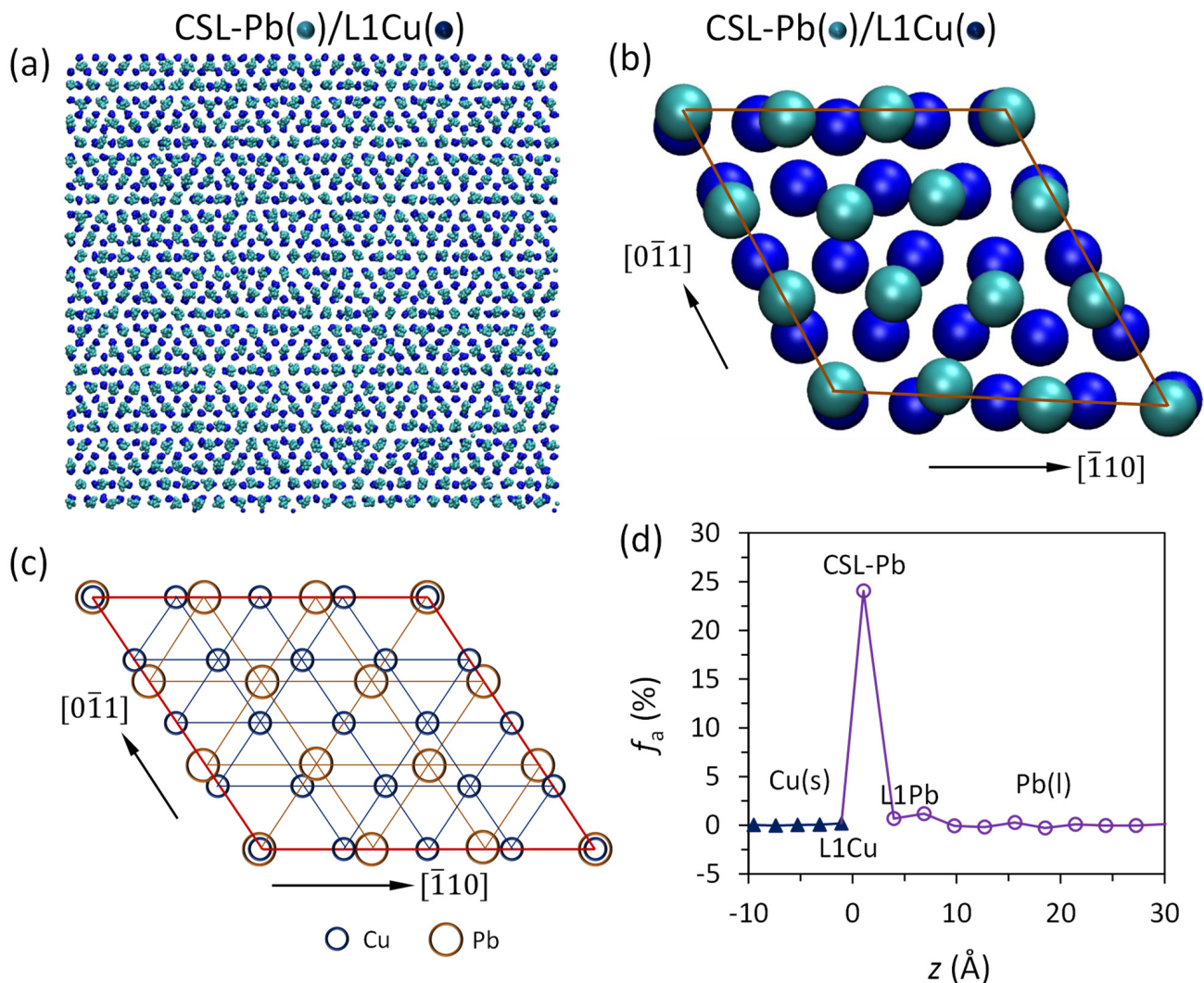
Prenucleation creates a coincidence site lattice (CSL) on the Cu substrate surface, and the CSL-Pb layer has become the new surface layer on top of the original Cu substrate (Figure 10a). The time-averaged atomic positions in the superimposed CSL-Pb/L1Cu layers exhibit a regular hexagonal pattern, which is too fine to be an edge dislocation network as observed in the systems with small negative misfit [18]. The relationship between CSL-Pb and L1Cu can be best described by a CSL: {111}<110>Pb // {111}<110>Cu and $3d_{Pb<110>} = 4d_{Cu<110>}$ matching of atomic spacings along the <110> directions on both {111}Pb and {111}Cu, where d is the atomic spacing along the <011> direction (Figure 10b,c). This is equivalent to the low-energy Σ7 CSL in the grain boundary [63].

The CSL formed during prenucleation accommodates a major part of the lattice misfit (Figure 10d) and transforms the original Cu substrate into a much more potent substrate (i.e., the CSL). Generally, if the amount of misfit accommodated by CSL is f_{CSL}, the residual misfit (f_r) can be expressed by the following equation:

$$f_r = f - f_{CSL}. \tag{4}$$

The calculated misfit accommodated by the CSL (f_{CSL}) is 25%, which accounts for a major part of the initial lattice misfit (27.3%) between solid Pb and Cu. Thus, the residual lattice misfit, f_r, is 2.3%. This indicates that the nucleation potency of the substrate with large lattice misfit can change fundamentally due to prenucleation.

For the subsequent heterogeneous nucleation, the CSL formed during prenucleation will be the new substrate, and the residual lattice misfit (f_r) becomes the only misfit relevant to the heterogeneous nucleation process.

Figure 10. Formation of coincidence site lattice (CSL) during prenucleation in the Pb(l)/Cu(s) system [27]. (**a**) Time-averaged atomic positions (top view) of the CSL layer (CSL-Pb) superimposed on that of L1Cu in the Pb(l)/Cu(s) system equilibrated at 625 K. (**b**) Snapshot of CSL-Pb/L1Cu showing atomic arrangement in the CSL unit cell; (**c**) the schematic illustration of CSL unit cell shows the matching rule, $3\,d_{Pb<110>} = 4\,d_{Cu<110>}$, where d is the atomic spacing along the <011> direction; and (**d**) the accommodated misfit, f_a, as a function of distance from the interface. The CSL accommodates a major part (25%) of the lattice misfit in the Pb(l)/Cu(s) systems, and only a small residual lattice misfit of 2.3% needs to be accommodated during the subsequent heterogeneous nucleation.

### 3.3.4. Prenucleation on Amorphous Substrates

Geysermans et al. [35] reported that the liquid Al exhibited a layered structure within six atomic layers adjacent to the amorphous Cu substrate with smooth surface, and did not display any layering to the bulk Cu amorphous substrate (3D amorphous substrates). We investigated the atomic ordering in the liquid Al adjacent to an amorphous Al substrate with either rough or smooth surfaces [64]. The amorphous substrates with smooth or rough surfaces are referred to as 2D or 3D amorphous substrates, respectively. Our study reveals that there exists a layered structure within four atomic layers in the liquid at the interface with 2D amorphous substrate (Figure 11a,b), and no layering for the 3D amorphous substrate (Figure 11c,d). This is consistent with the findings of Geysermans et al. [35] and the previous study in our group [25]. It further confirms that the layering is attributed to the "hard wall" effect, and will disappear as soon as the "hard wall" is missing.
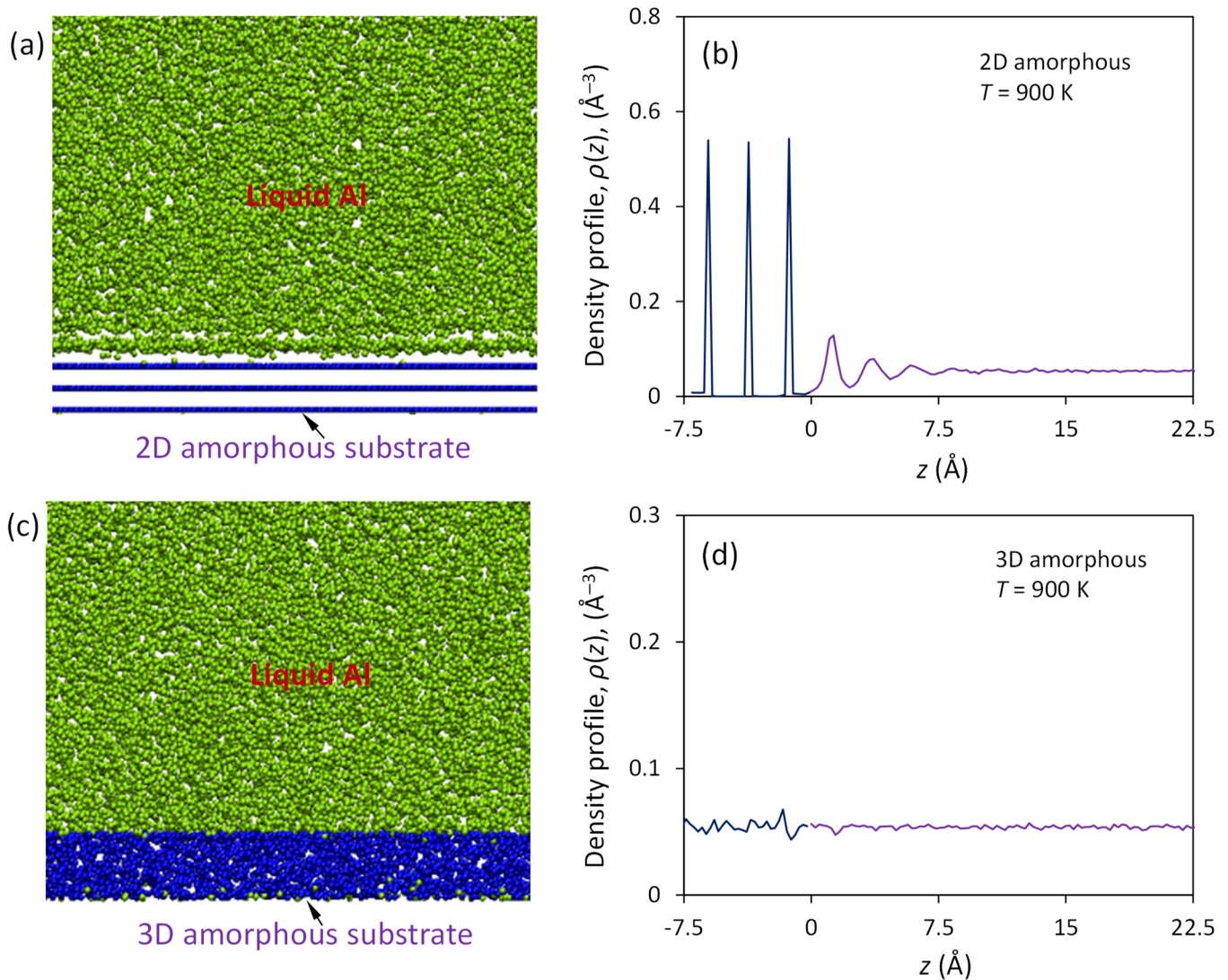
Figure 11. Atomic ordering at liquid/amorphous substrate interface [64]. Front view of a partial snapshot of the liquid Al/amorphous substrate system with (**a**) atomically smooth amorphous substrate surface (2D amorphous substrate) and (**c**) atomically rough amorphous substrate surface (3D amorphous substrate). The system was equilibrated at T = 900 K. The atomic density profile, $\rho(z)$, is plotted as a function of the distance from the interface for the system with (**b**) 2D amorphous substrate and (**d**) 3D amorphous substrate. The liquid exhibits layering within the first four atomic layers in the liquid at the interface with 2D amorphous substrate, and no layering in the system with 3D amorphous substrate.

An amorphous substrate with a smooth surface can induce prenucleation, as revealed by the time-averaged atomic positions of the surface layer of the substrate (A1), L1/A1, L2, and L3 in the simulation system with 2D amorphous substrate at t = 100 ps during the simulation at T = 579 K (Figure 12). We found that the nucleation temperature of liquid Al on a 2D amorphous substrate is 579 K. There are ordered regions in L1 and L2 (Figure 12b,c), indicative of the existence of a 2D ordered structure in the liquid at the interface prior to nucleation. Further analysis suggests that local short-range order exists in the amorphous substrate with a smooth surface, which induces local ordered structure in the liquid. This suggests that prenucleation exists in the liquid at the interface even with an amorphous substrate with a smooth surface, and the structural templating mechanism is responsible for the prenucleation in such cases.
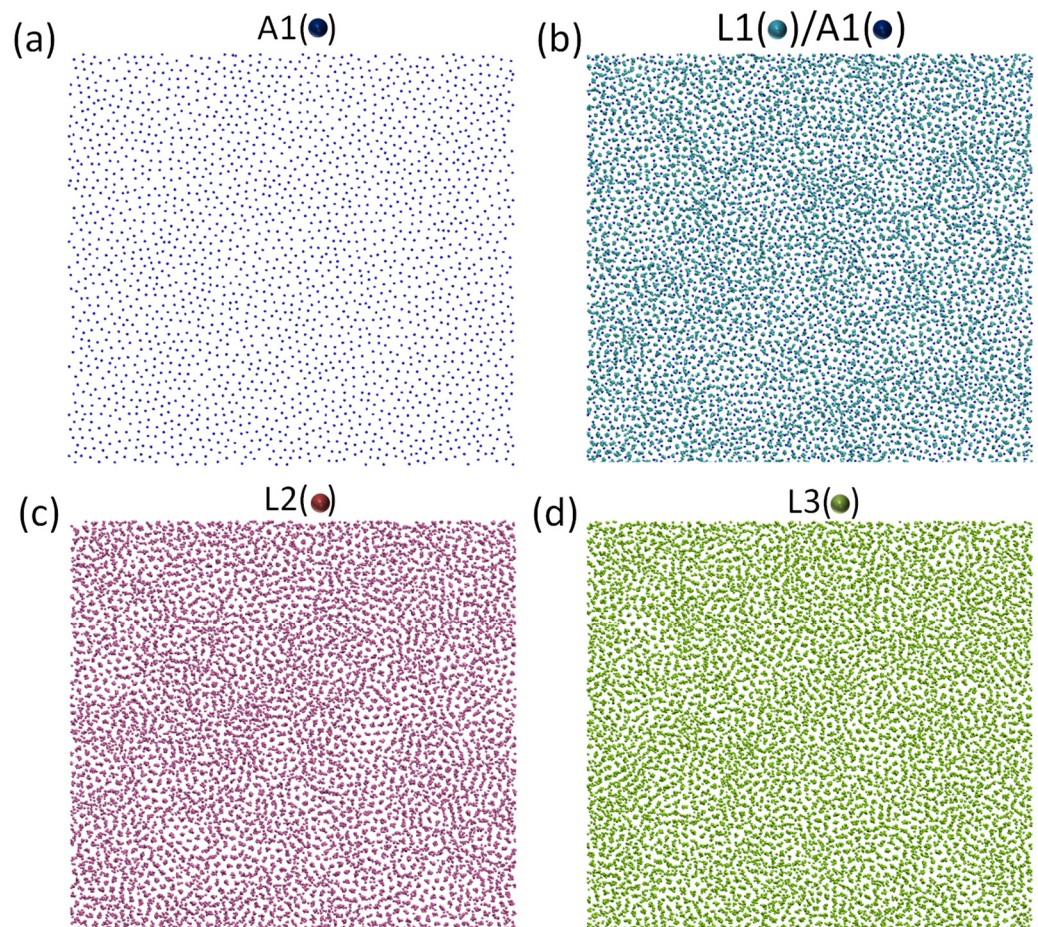
Figure 12. Local ordered structure in the liquid at the liquid/amorphous substrate with a smooth surface [64]. Time-averaged atomic positions of (**a**) A1, (**b**) L1/A1, (**c**) L2, and (**d**) L3 for the simulation system with 2D amorphous substrate at t = 100 ps during the simulation at T = 579 K. The local short-range order in the amorphous substrate can template solid clusters in the liquid at the interface with the smooth surface of the amorphous substrate.

3.4. Effect of Chemistry

To examine the effect of the chemistry, ab initio MD simulations were performed for the systems of liquid Al with pinned Ag, W, Al, or Cd substrates (denoted as L-Al/S-Ag, L-Al/S-W, L-Al/S-Al, L-Al/S-Cd, respectively) [26], using the VASP within the projector-augmented wave (PAW) framework [65,66] and the generalised gradient approximation, formulated by Perdew, Burke, and Ernzerhof (PBE) [67]. The liquid Al atoms have an attractive interaction with the Ag and W substrates, a neutral interaction with the Al substrate, and a repulsive interaction with the Cs substrate. The heat of mixing, ΔH_{mix}, is −4.0 kJ/mol, −2.0 kJ/mol, 0 and 3.0 kJ/mol, respectively, for the Al/Ag, Al/W, Al/Al, and Al/Cd systems. We constructed the substrates of Ag, W, Al, or Cd with the same configuration and lattice parameter as that of fcc Al. Thus, all such substrates have the same crystal structure and the same lattice parameter as that of the solid Al (hence 0 lattice misfit), but with different chemical characteristics. By doing so, we can investigate the effect of substrate chemistry on prenucleation without the interference of substrate structures.

Prenucleation at the interface could become more complicated if the effect of the chemistry is considered, where the atoms are subject to attractive or repulsive interactions, respectively, from the substrate if there is a negative or positive heat of mixing between the substrate and liquid atoms. We found that for a given liquid, an attractive chemical interaction (negative heat of mixing) strengthens atomic ordering at the interface, and a repulsive interaction (positive heat of mixing) weakens atomic ordering. The atoms

in the liquid at the interface exhibit stronger atomic layering for the L-Al/S-Ag system (Figure 13a), and weaker atomic layering for the L-Al/S-Cd system (Figure 13c), compared to that for the L-Al/S-Al system (Figure 13b).
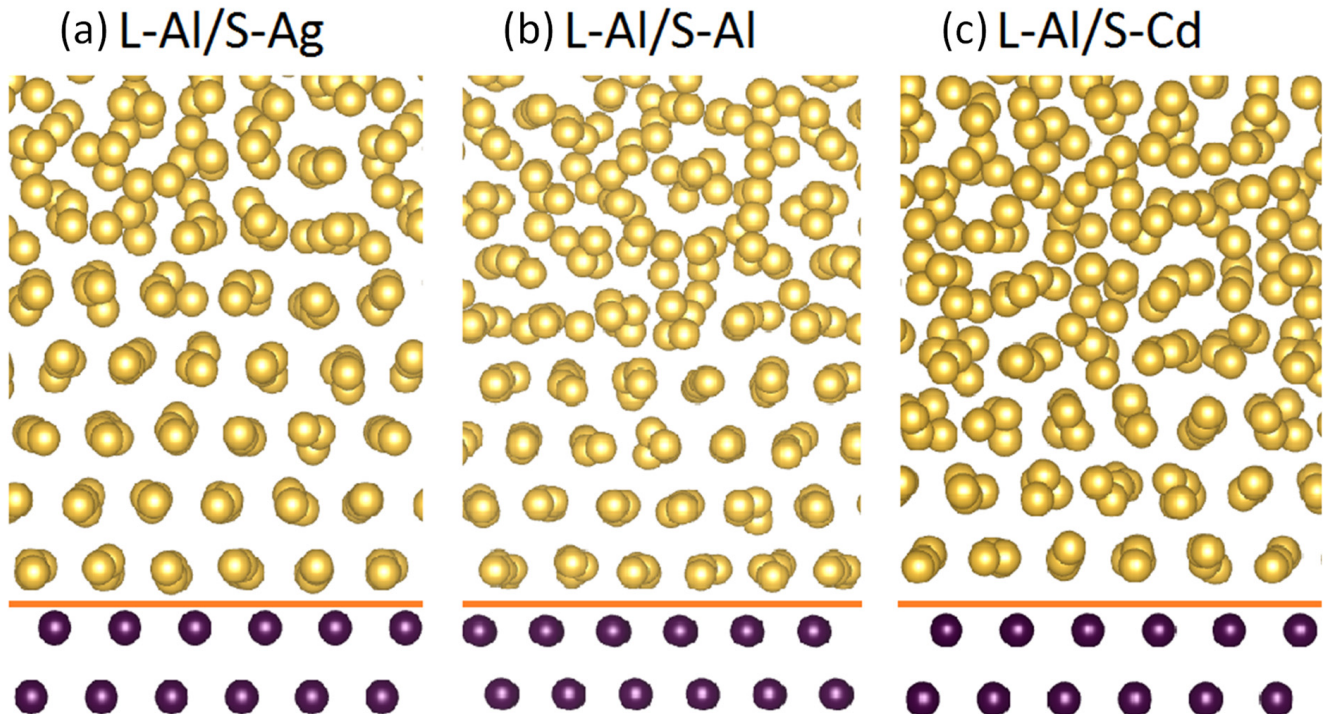
Figure 13. Chemistry effect on prenucleation at the liquid/substrate interface [26]. Snapshots of the simulation systems of the liquid Al and pinned substrate: (**a**) L-Al/S-Ag, (**b**) L-Al/S-Al, and (**c**) L-Al/S-Cd systems. All systems were equilibrated at 1000 K. The violet and light gold spheres represent the substrate and liquid atoms, respectively, and the solid orange lines mark the Gibbs dividing interface between the substrate and the liquid.

Atomic ordering at the interface degrades monotonically with the transition from attractive to repulsive interactions between the liquid and substrate atoms, while the structure effect is excluded (Figure 14). With the decrease of ΔH_{mix} from positive to negative, the peak density ($\rho(z)_{\mathrm{L1}}$) and in-plane ordering ($S_{\mathrm{L1}}(z)$) in L1, and the number of atomic layers (n_{L}) at the interface increase linearly (Figure 14a–c), and interlayer spacing (d_{L1}) between L1 and the substrate decreases linearly (Figure 14b). This suggests that an attractive chemical interaction between the liquid and substrate atoms increases the bond strength between the atoms in the first layer of the liquid and the surface layer of the substrate. Consequently, the atoms in the first layer of the liquid are further confined to their equilibrium atomic positions provided by the surface layer of the substrate. This strengthens structural templating, and hence increases the atomic ordering at the liquid/substrate interface. On the other hand, the repulsive interaction decreases the bond strength between the atoms in the first layer of the liquid and the surface layer of the substrate, and the atoms in the first interfacial layer are pushed away from the equilibrium atomic positions provided by the substrate. This weakens the structural templating, and hence impedes the atomic ordering at the interface. It should be pointed out that the structural effect of the substrate dominates the atomic ordering. The chemical effect is a secondary factor, and affects the atomic ordering through either strengthening or weakening the structural templating [26].
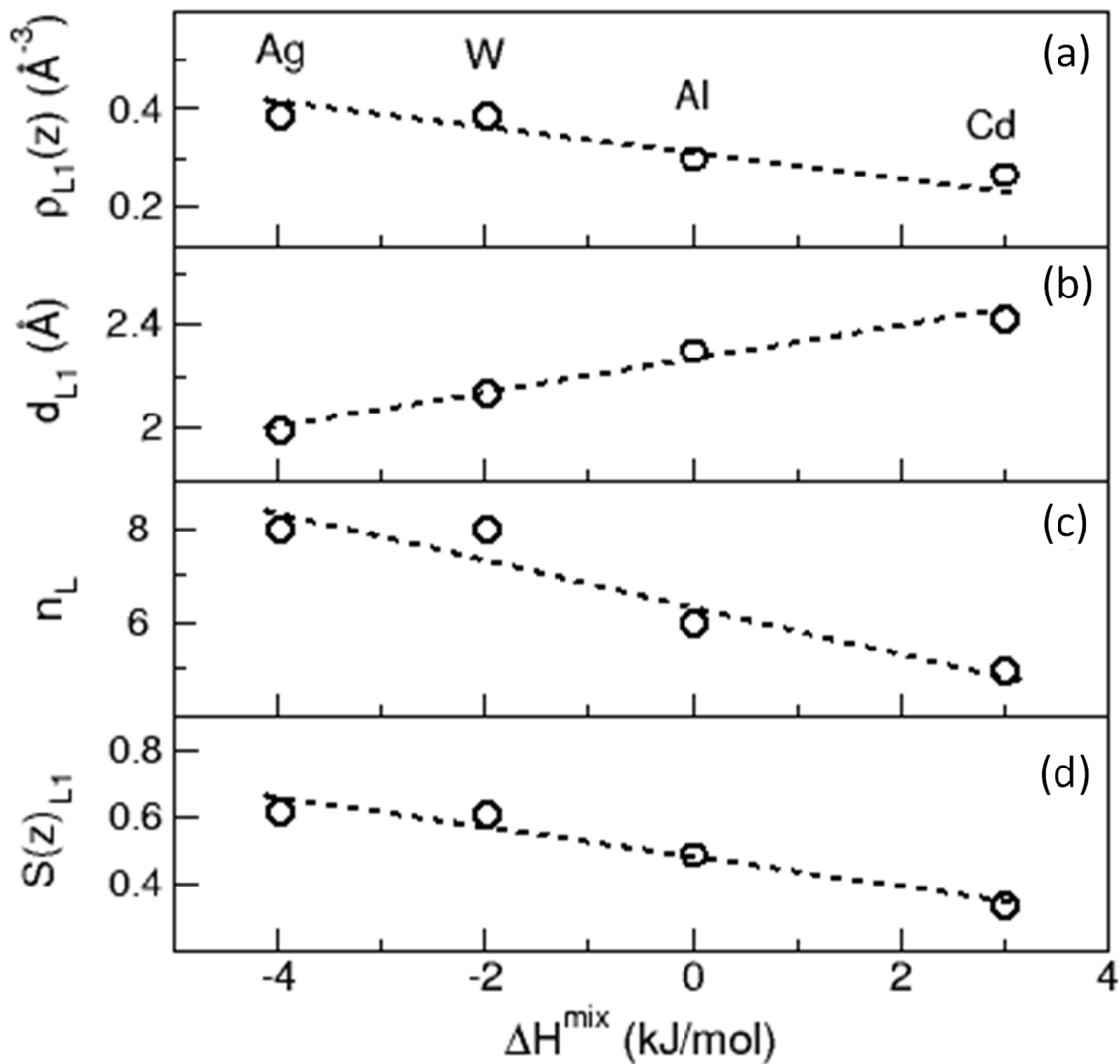
Figure 14. Chemistry effect on atomic ordering at the liquid/substrate interface [26]. (**a**) Peak density of L1, $\rho_{L1}(z)$, (**b**) interlayer spacing of L1, d_{L1}, (**c**) number of interfacial layers, n_L, and (**d**) in-plane atomic order parameter of L1, $S(z)_{L1}$, are plotted as a function of the heat of mixing, ΔH_{mix}, between the liquid Al and the substrate atoms for the systems of L-Al/S-Ag, L-Al/S-W, L-Al/S-Al, and L-Al/S-Cd, equilibrated at 1000 K. The atomic ordering in the liquid at the interface degrades monotonically with the transition from the attractive to repulsive interaction between the liquid and the substrate.
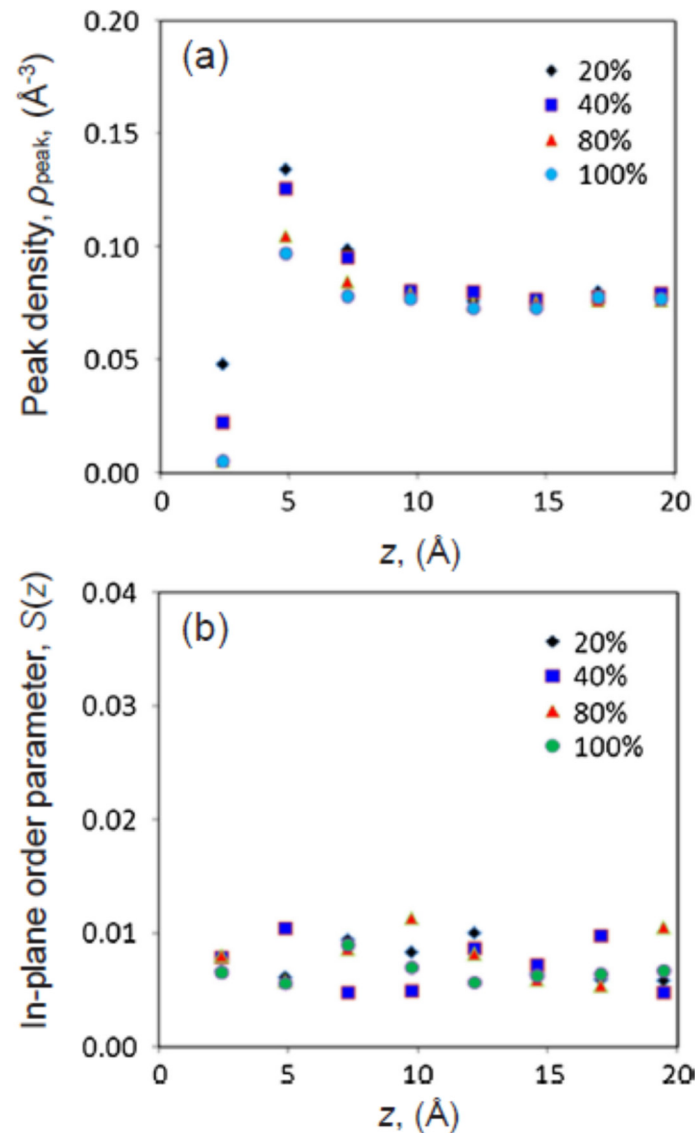
3.5. Effect of Substrate Roughness

To examine the effect of the surface roughness of the substrate at the atomic level, classical MD simulations were conducted for the systems of liquid Al/fixed substrate [25], where the substrate is either crystalline or amorphous with varied surface roughness at the atomic level. The RGL potential, created by Rosato, Guillope, and Legrand [68], was used in the simulations.

3.5.1. Amorphous Substrate

Geysermans et al. [35] found that the atomic layering is suppressed by the surface roughness of an amorphous substrate, and even destroyed completely by the rough surface of a bulk amorphous substrate. We investigated the atomic ordering in the liquid Al adjacent to amorphous Al substrates with varied atomic-level surface roughness [25]. The atomic level surface roughness, R, is defined as: $R = \Sigma(\Delta h_i)/nh \times 100\%$, where Δh_i is the displacement of the ith atom away from a smooth reference plane; h is the spacing of a

smooth reference plane; n is the total number of atoms in the layer; and $\Delta h_i < h$ to confine surface roughness to an atomic scale. For a bulk amorphous substrate, no layered structure was observed at the interface. The atomic layering in the liquid at the interface reduces with an increase in the surface roughness of an amorphous substrate (Figure 15a). This is consistent with the observation of Geysermans et al. [35].

Figure 15. Effect of surface roughness of the amorphous substrate on atomic ordering [25]. (**a**) $\rho_P(z)$ and (**b**) $S(z)$ of the liquid Al adjacent to the interface are plotted as functions of distance from the interface and surface roughness, R, in the simulation system with a single layer of amorphous substrate, equilibrated at 1000 K. L1 has a relatively low peak density, which accounts for the liquid atoms occupying a fraction of the atomic positions in the surface layer of the substrate. The layering of the liquid at the interface deteriorates with increasing R, and there is no visible in-plane atomic ordering regardless of R. (Reprinted with permission from Ref. [25]. Copyright 2022, Elsevier.)

The liquid adjacent to a bulk amorphous substrate exhibits a disordered structure (Figure 16a–d), indicating that these atoms have the same characteristics as the bulk liquid. The amorphous substrate can almost completely eliminate the in-plane ordering in the liquid regardless of its surface roughness (Figure 15b). The value of $S(z)$ is close to or below 0.01 for all of the interfacial atomic layers, which is approximately the value of $S(z)$ for the bulk liquid. It can be concluded that the atomic layering in the liquid at the interface

is impeded substantially by the increasing surface roughness of an amorphous substrate, and the in-plane atomic ordering is eliminated by an amorphous substrate regardless of surface roughness.
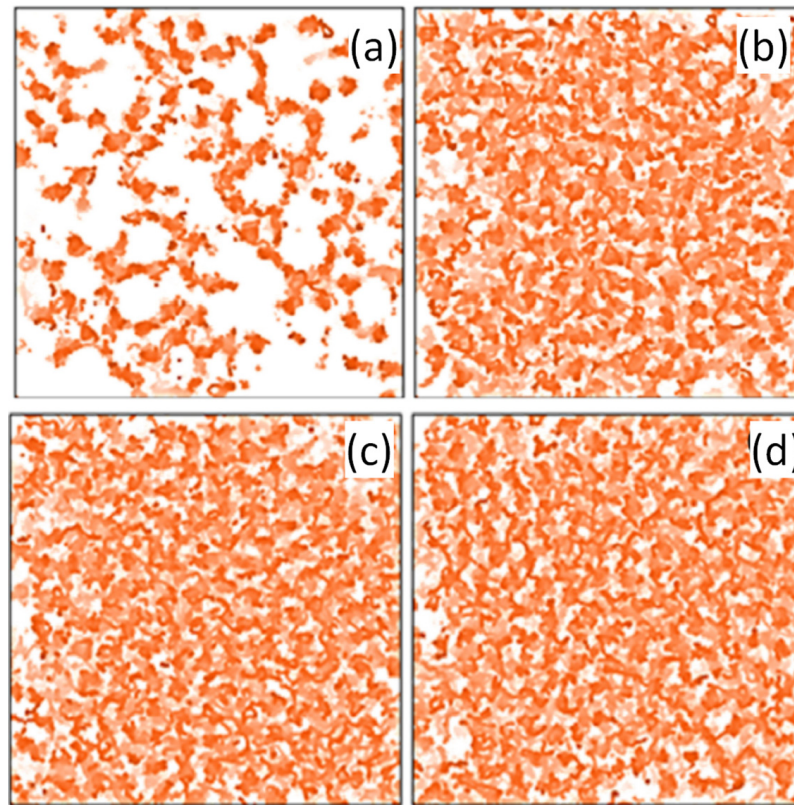

Figure 16. Atomic ordering at the interface of liquid/bulk amorphous substrate [25]. The time-averaged atomic positions of (**a**) L1, (**b**) L2, (**c**) L3, and (**d**) L4 in the liquid Al adjacent to the bulk amorphous substrate equilibrated at 1000 K. The atoms in the liquid at the interface exhibit a completely disordered structure. (Reprinted with permission from Ref. [25]. Copyright 2022, Elsevier.)

3.5.2. Crystalline Substrate

We also investigated the atomic ordering in the liquid Al adjacent to a crystalline substrate with varied atomic-level surface roughness. The rough crystalline substrate is artificially constructed from an fcc Al substrate with a <111> surface orientation, where the smooth reference plane is the {111} plane of the fcc Al with the roughness $R = 0$. The liquid Al adjacent to a smooth crystalline substrate ($R = 0$ and 0% misfit) equilibrated at 1000 K exhibits a layered structure within five atomic layers at the interface. There is a nearly ordered structure in L1, a mixed structure with ordered and disordered regions in L2 and L3, and a disordered structure in L4. This is in a good agreement with our result in Section 3.1.1.

With the increasing surface roughness of a crystalline substrate, both atomic layering and in-plane atomic ordering in the metallic liquid at the interface are significantly reduced (Figure 17). The ρ_p of L1 decreases dramatically with increasing surface roughness, and the decrease in ρ_p becomes less dramatic for the subsequent layers (Figure 17a). The layering becomes negligible for large surface roughness. The in-plane ordering of the liquid at the interface also deteriorates dramatically with increasing surface roughness (Figure 17b). Significant in-plane ordering exists within the first two atomic layers for small surface roughness, e.g., $R < 30\%$. With the further increase in surface roughness, the in-plane atomic ordering at the interface decreases substantially. At a large surface roughness, the in-plane atomic ordering becomes negligible even for the first liquid layer.

It was demonstrated that the atomic ordering at the interface can be demolished partially or almost completely by impeding the "hard wall" effect and/or structural templating with a rough substrate [25]. For an atomically rough surface of the crystalline substrate, both the "hard wall" effect for atomic layering and the structural templating for in-plane atomic ordering are impeded. As expected, the atomic layering and in-plane atomic ordering decrease with an increase of the surface roughness of a crystalline substrate [25]. For the rough surface of an amorphous substrate, structural templating for in-plane atomic ordering is impeded almost completely due to the disordered structure of the substrate, and the "hard wall" effect for the atomic layering is gradually impeded with increasing the surface roughness of the substrate. Thus, the rough surface of an amorphous substrate almost completely eliminates in-plane atomic ordering in the liquid regardless of surface roughness, and reduces/eliminates the atomic layering depending on the surface roughness [25].
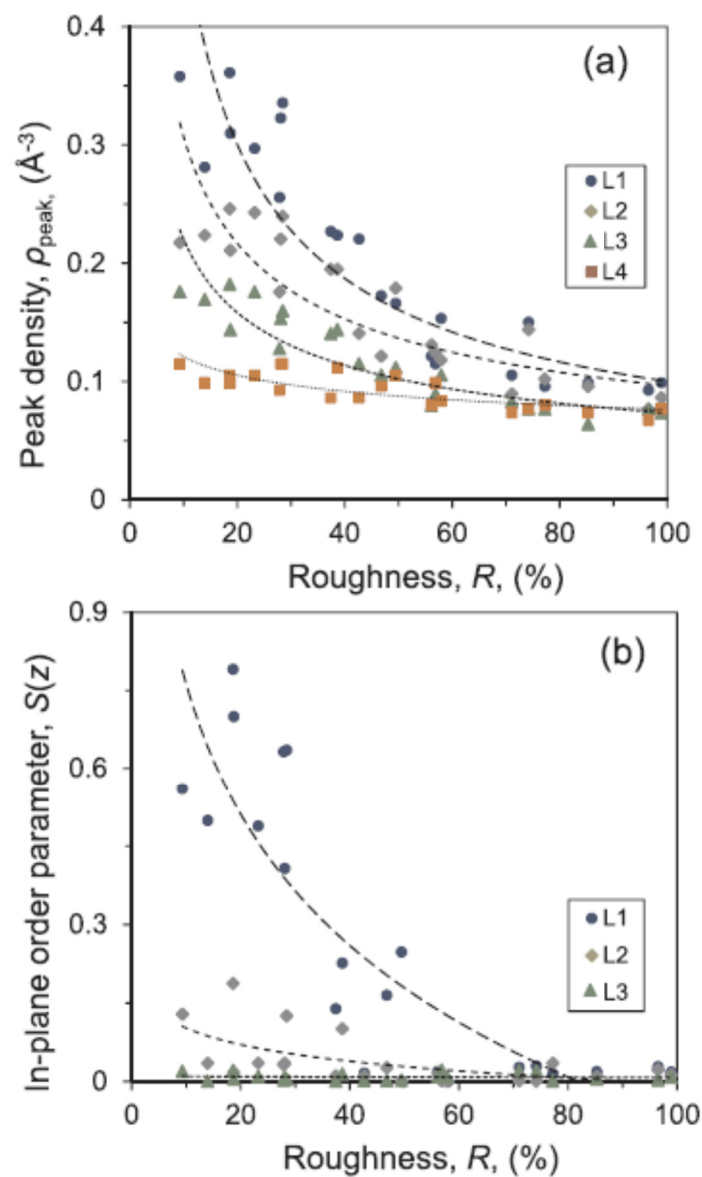
Figure 17. Effect of surface roughness of crystalline substrate on prenucleation [25]. (**a**) $\rho_P(z)$ and (**b**) $S(z)$ of L1, L2, L3, and L4 in liquid Al adjacent to a crystalline substrate as a function of surface roughness, R, equilibrated at 1000 K. The dashed lines are the fitting line for each data set. Both the layering and in-plane ordering adjacent to the interface deteriorate with increasing surface roughness, R. (Reprinted with permission from Ref. [25]. Copyright 2022, Elsevier.)

3.6. Prenucleation at Liquid/Oxide Interface

During the liquid handling and casting of Mg and Al alloys, oxide particles, including magnesia (MgO), (α- and γ-) alumina (Al_2O_3), and spinel ($MgAl_2O_4$), are formed inevitably in the alloy melts. Experimental observations revealed that the native MgO particles in liquid Mg alloys are dominant with {111} facets [69], α-Al_2O_3 with {0001} facets, and γ-Al_2O_3 with {111} facets in Al-melts [70], and $MgAl_2O_4$ with {111} facets in Al-Mg alloys [70]. It is generally accepted that these native oxide particles have harmful effects on the mechanical performance of the cast components [71]. However, they may be harnessed to act as heterogeneous nucleation sites during solidification to deliver significant grain refinement without the need for grain refiner addition [70,72,73].

We used parameter-free ab initio molecular dynamics (AIMD) approaches to investigate the prenucleation at the interfaces between liquid metals and oxides, including systems of L-Mg/MgO{111} [74], L-Al/MgO{111} [75,76], L-Al/α-Al_2O_3{0001} [75], L-Al/γ-Al_2O_3{111} [77], and L-Al/$MgAl_2O_4${111} [78]. Chemically, these oxides are ionic compounds due to the large differences in the electronegativity values of the metals (1.61 for Al, 1.31 for Mg in Pauling scale) and the oxygen (3.44). For example, in γ-Al_2O_3, all of the oxygen ions have an average charge value of -1.3 e/O, whereas the Al are positively charged ($+2.0$ e/Al). Our study reveals [77] that the charge transfer occurs from the atoms of the first interfacial Al layer to the outmost O atoms. The atoms in the first interfacial Al layer are positively charged and bonded to the outmost O layer of the substrate, and thus become chemically an integral part of the substrates or new terminating layer of the oxides in the melt. The γ-Al_2O_3 has a defective spinel-type structure [79]. Along its [111} axis, it consists of an alternating oxygen layer and Al layer. There are two types of Al layers: one is composed of three Al sublayers (denoted as γ-Al_2O_3{111}Al_1) and the other comprises a flat Al layer (denoted as γ-Al_2O_3{111}Al_2). The newly formed Al layer is smooth at the L-Al/γ-Al_2O_3{111}Al_2 interface, while it is atomically rough at the L-Al/γ-Al_2O_3{111}Al_1 interface. The liquid Al atoms are well separated from the substrate at the L-Al/γ-Al_2O_3{111}Al_2 interface, whereas there is no clear border between the liquid Al atoms and the substrate at the L-Al/γ-Al_2O_3{111}Al_1 interface. It exhibits moderate atomic ordering at the first Al layer, but little at the second Al layer at the L-Al/γ-Al_2O_3{111}Al_2 interface. At the L-Al/γ- Al_2O_3{111}Al_1 interface, on the other hand, even the first Al layer displays hardly any atomic ordering. In addition, the L-M/oxide interfaces exhibit a range of lattice misfits from moderate (0.4%) to high (7.9%), with a similar degree of layering [77].

It is worthwhile to note that the layering at the L-M/oxide interfaces is notably weaker than that at the L-M/S-M interface [18,26]. For instance, the layering at the L-M/S-M interface usually persists within about six atomic layers [18], and the L-Al/MgO{111}$_{Mg}$ interface has four recognisable layers with the in-plane ordering coefficient of 0.18 in the first layer [75].

3.7. Manipulation of Substrate Potency by Interfacial Segregation

In reality, there are always some solute or impurity atoms in the melts. They may segregate to the liquid/substrate interface driven by the reduction of interfacial energy, according to the Gibbs adsorption rule [80]. The epitaxial nucleation model [11] suggests that a reduction of the interfacial energy by segregated solute elements at the interface can be achieved by:

- Reaction with the solvent to form an intermetallic phase on the substrate;
- Reaction with the substrate to form a new compound on the substrate;
- Segregation at the interface to influence the lattice parameter of the solid phase;
- Dissolution into the substrate to change the lattice parameter of the substrate.

Therefore, the physical properties (i.e., lattice misfit, surface roughness) of the substrate and the chemistry at the interface will be altered by the solute segregation. It, in turn, affects the prenucleation at the interface and the potency of the substrate. For instance, a solute element will enhance heterogeneous nucleation if it reduces the misfit, and impedes heterogeneous nucleation if it increases the misfit. Thus, we can manipulate the potency of

the substrate by selecting a nucleating substrate and segregation of some solute elements in such a way that nucleation is either enhanced or impeded through prenucleation.

Our recent experimental works demonstrated that the potency of the substrate could be effectively manipulated, either enhanced or impeded, by the chemical segregation of selected alloying/impurity elements at the liquid/substrate interface. For instance, Al–Ti–B is the most widely used grain refiner for many Al alloys. Our high-resolution electron microscopy investigation confirmed the existence of a Ti-rich monolayer on the (0001) TiB_2 surface due to the segregation of Ti, which is most likely to be a (112) Al_3Ti two-dimensional compound (2DC) [81,82]. The potency of TiB_2 particles is significantly increased by the formation of a monolayer of Al_3Ti 2DC on their surface in concentrated Al–Ti solutions. On the other hand, the effectiveness of such grain refiners is severely compromised when a few hundred ppm of Zr are present in the Al melt, known as Zr poisoning in the literature [83]. The presence of Zr in Al melts leads to (i) the dissolution of the Al_3Ti 2DC on the (0001) TiB_2 surface due to the segregation of Zr; and (ii) the formation of an atomic monolayer of Ti_2Zr 2DC on the (0001) TiB_2 surface. This monolayer of Ti_2Zr not only has a large lattice misfit (-4.2%) with α-Al, but is also atomically rough, rendering the TiB_2 particles impotent for the heterogeneous nucleation of α-Al.

4. Discussion

4.1. Prenucleation Describes the Phenomenon of Substrate-Induced Interfacial Atomic Ordering

Our studies revealed that the physical and chemical properties of the substrate have significant effects on the atomic ordering in the liquid at the interface, and a 2D ordered structure may be induced by the substrate through a structural templating mechanism. We confirmed that atomic layering can extend up to six atomic layers at the interface at temperatures close to the liquidus, and the in-plane atomic ordering may persist within the first three atomic layers at the interface of a crystalline substrate with very small lattice misfit, agreeing well with the literature [14–16,35]. We found that the atomic layering was independent of lattice misfit, and was only slightly enhanced by reducing the temperature [18,24]. On the other hand, the degree of in-plane atomic ordering is significantly enhanced by reducing the temperature and/or lattice misfit [18,24]. The 2D ordered structure in the liquid at the interface changes significantly with the physical and chemical properties of the substrate. This concept of prenucleation contrasts with the hypernucleation hypothesis [84,85], which suggested that a few atomic layers of quasi-solid Al containing Ti could form on the (0001) TiB_2 surface in the Al melts even above the melting temperature. Such quasi-solid layers could become a precursor for the formation of the new phase at a very small undercooling [86,87]. However, the existence of such a quasi-solid at the interface may be thermodynamically unstable in dilute Al–Ti melts at temperatures above T_1. In addition, the recent experimental observation with SuperSTEM [82] also does not support this hypothesis, which revealed that only a single layer of 2D compound, (112) Al_3Ti, formed on the (0001) TiB_2 surface through chemical adsorption. An adsorbed monoatomic layer would be stable at the interface if the liquid/substrate interfacial energy is reduced [88]. In this case, the free energy increase due to the formation of the 2DC at the interface is compensated by the interfacial energy reduction. The formation of the 2D ordered structures during prenucleation is driven by the reduction of the liquid/substrate interfacial energy, and thus is thermodynamically favourable.

4.2. Prenucleation Provides a Precursor for Heterogeneous Nucleation

Our MD simulation results (Figure 3) confirmed that the atomic ordering in the liquid at the liquid/substrate interface increases with decreasing temperature, and this trend continues beyond the liquidus until the nucleation temperature is reached. This suggests that at lower temperatures, the substrate has a higher capability to template atomic ordering in the liquid due to the reduced atomic mobility and larger driving force. Prior to the onset of heterogeneous nucleation at the nucleation temperature (T_n), prenucleation reaches its maximum in terms of the fraction of solid atoms at the liquid/substrate interface [89],

which provides a precursor for the heterogeneous nucleation process. This precursor represents the maximum atomic ordering at the liquid/substrate interface and serves as a starting point for heterogeneous nucleation at T_n. Our research on heterogeneous nucleation processes [89] revealed that although heterogeneous nucleation in systems with varying lattice misfits occurred at different nucleation temperatures, with T_n decreasing linearly with increasing lattice misfit, it always started with the same precursor with the same level of atomic ordering [89]. On one hand, at the same temperature, atomic ordering at the liquid/substrate interface decreases with increasing lattice misfit; on the other hand, for a given system, the nucleation temperature decreases with increasing lattice misfit. The overall outcome of the interplay between temperature and lattice misfit is that systems with different lattice misfits will start with the same precursor. This is a good demonstration of the importance of prenucleation in heterogeneous nucleation.

4.3. Prenucleation Leads to the Lowest γ_{LN} at the Nucleation Temperature

We calculated the interfacial energy, γ_{LN}, of the liquid/substrate interface as a function of the fraction of ordered atoms in the interface and found that γ_{LN} decreases with the increasing fraction of ordered atoms in the interface [89,90]. By ignoring the chemical interaction between the substrate and the liquid, the interfacial energy of the liquid/substrate interface, γ_{LN}, is closely related to the number of ordered atoms in the diffuse interface. At a given temperature, γ_{LN} decreases with the increasing number of interfacial solid atoms. For a given temperature, the number of ordered atoms in the L/N interface decreases and γ_{LN} increases with increasing misfit. However, the increase in misfit leads to a decrease in T_n, which in turn causes the increase in atomic ordering in the L/N interface at T_n. The overall effect of increasing misfit is that systems with different misfit have the same atomic ordering in the L/N interface and thus the same γ_{LN} at their respective nucleation temperatures [89]. This suggests that heterogeneous nucleation in systems with different misfits occurs at different temperatures, but with the same atomic ordering in the L/N interface. In other words, heterogeneous nucleation always starts with the same precursor, with the lowest interfacial energy (γ_{LN}) [89,90].

4.4. Prenucleation Originates Physically from Structural Templating

Atomic layering can be attributed to the "hard wall" effect of the substrate [49,50], and is therefore independent of the crystal structure [14,16,17], surface orientation [15,35], and lattice parameter [18,24,27] of the substrate. We found that in-plane atomic ordering resulted from the structural templating. The surface lattice of the substrate provides low-energy positions for atoms in the first layer of the liquid. The occupancy of such low-energy atomic positions depends largely on the crystallographic matching between the substrate and the solidified phase from the liquid, which is quantified by the lattice misfit. Our study revealed that there exists an epitaxial interface for either small negative lattice misfit [18] or small positive lattice misfit [24]. For systems with large lattice misfit, the interface is also epitaxial due to the formation of the CSL during prenucleation [27]. Therefore, if heterogeneous nucleation does occur, a specific orientation relationship always exists between the solid and the substrate for a full range of lattice misfit. This suggests that structural templating plays a critical role in prenucleation, and that it will continue to play a critical role during both heterogeneous nucleation [91] and the subsequent crystal growth processes [90].

5. Summary

The physical and chemical properties of the substrate have a significant effect on the atomic ordering in the liquid at the liquid/substrate interface. We have developed the concept of prenucleation to describe the substrate-induced atomic ordering in the liquid at the liquid/substrate interface at temperatures above the nucleation temperature. Using classical MD and ab initio DFT simulations, we systematically investigated the effects of temperature, lattice misfit, substrate surface roughness, and the chemical interaction

between the substrate and the liquid on prenucleation. The main findings are summarised as follows:

- Prenucleation describes the phenomenon of substrate-induced atomic ordering in the liquid at the liquid/substrate interface at temperature above the nucleation temperature.
- Prenucleation can be described in three different ways depending on the purpose of analysis: (1) atomic layering and in-plane atomic ordering for quantifying the substrate induce atomic ordering; (2) two-dimensional order structure at the liquid/substrate interface for describing the interfacial atomic arrangement; and (3) a diffuse liquid/substrate interface for linking interfacial atomic ordering with interfacial energies.
- Prenucleation is promoted by reducing the temperature, lattice misfit, or atomic-level surface roughness and by having an attractive chemical interaction between the substrate and liquid atoms.
- The physical origin of in-plane atomic ordering during prenucleation is structural templating by the substrate lattice, while that of atomic layering is the "hard wall" effect.
- While structural templating dictates prenucleation, the chemistry effect is a secondary factor in determining the atomic ordering at the liquid/substrate interface. An attractive chemical interaction strengthens structural templating, and a repulsive interaction weakens it.
- Atomic ordering at the liquid/substrate interface can be demolished by impeding the "hard wall" effect and/or structural templating with an atomically rough substrate surface. Increasing the surface roughness of a crystalline substrate reduces both atomic layering and in-plane atomic ordering.
- The rough surface of an amorphous substrate can eliminate in-plane ordering in the liquid at the liquid/substrate interface, resulting in such a substrate having no structural templating power.
- The nucleation potency of a substrate can be manipulated by the segregation of selected elements at the liquid/substrate interface in such a way that nucleation is either enhanced or impeded through prenucleation.

References

1. Kelton, K.F.; Greer, A.L. *Nucleation in Condensed Matter: Applications in Materials and Biology*; Elsevier Science: Oxford, UK, 2010.
2. Kashchiev, D. *Nucleation: Theory with Applications*; Butterworth-Heinemann: Oxford, UK, 2000.
3. Bartels-Rausch, T. Chemistry: Ten things we need to know about ice and snow. *Nature* **2013**, *494*, 27–29. [CrossRef] [PubMed]
4. Sosso, G.C.; Chen, J.; Cox, S.J.; Fitzner, M.; Pedevilla, P.; Zen, A.; Michaelides, A. Crystal nucleation in liquids: Open questions and future challenges in molecular dynamics simulations. *Chem. Rev.* **2016**, *116*, 7078–7116. [CrossRef] [PubMed]
5. Greer, A.L. Overview: Application of heterogeneous nucleation in grain-refining of metals. *J. Chem. Phys.* **2016**, *145*, 211704. [CrossRef] [PubMed]
6. Erdemir, D.; Lee, A.Y.; Myerson, A.S. Polymorph selection: The role of nucleation, crystal growth and molecular modelling. *Curr. Opin. Drug Discov. Devel.* **2007**, *10*, 746–755.
7. Michaels, T.C.T.; Šarić, A.; Curk, S.; Bernfur, K.; Arosio, P.; Meisl, G.; Dear, A.J.; Cohen, S.I.A.; Dobson, C.M.; Vendruscolo, M.; et al. Dynamics of oligomer populations formed during the aggregation of Alzheimer's Aβ42 peptide. *Nat. Chem.* **2020**, *12*, 445–451. [CrossRef]

8. Easton, M.A.; Qian, M.; Prasad, A.; StJohn, D.H. Recent advances in grain refinement of light metals and alloys. *Curr. Opin. Solid State Mater. Sci.* **2016**, *20*, 13–24. [CrossRef]
9. Kaplan, W.D.; Kauffmann, Y. Structural order in liquids induced by interfaces with crystal. *Annu. Rev. Mater. Res.* **2006**, *36*, 1–48. [CrossRef]
10. Asta, M.; Spaepen, F.; van der Veen, J.F. Solid-liquid interfaces: Molecular structure, thermodynamics, and crystallization. *MRS Bull.* **2004**, *29*, 920–926. [CrossRef]
11. Fan, Z. An epitaxial model for heterogeneous nucleation on potent substrates. *Metall. Mater. Trans. A* **2013**, *44*, 1409–1418. [CrossRef]
12. Oh, S.H.; Kauffmann, Y.; Scheu, C.; Kaplan, W.D.; Rühle, M. Ordered liquid aluminium at the interface with sapphire. *Science* **2005**, *310*, 661–663. [CrossRef]
13. Oh, S.H.; Scheu, C.; Rühle, M. In-situ HRTEM studies of alumina-aluminium solid-liquid interfaces. *Korean J. Electron Microsc. Spec. Issue* **2006**, *1*, 19–24.
14. Hashibon, A.; Adler, J.; Finnis, M.W.; Kaplan, W.D. Ordering at solid-liquid interfaces between dissimilar materials. *Interface Sci.* **2001**, *9*, 175–181. [CrossRef]
15. Hashibon, A.; Adler, J.; Finnis, M.W.; Kaplan, W.D. Atomistic study of structural correlations at a liquid-solid interface. *Comp. Mater. Sci.* **2002**, *24*, 443–452. [CrossRef]
16. Palafox-Hernandez, J.P.; Laird, B.B.; Asta, M. Atomistic characterization of the Cu-Pb solid-liquid interface. *Acta Mater.* **2011**, *59*, 3137–3144. [CrossRef]
17. Wang, J.S.; Horsfield, A.; Schwingenschlögl, U.; Lee, P.D. Heterogeneous nucleation of solid Al from the melt by Al_3Ti: Molecular dynamics simulations. *Phys. Rev. B* **2010**, *82*, 184203.
18. Men, H.; Fan, Z. Prenucleation induced by crystalline substrates. *Metall. Mater. Trans. A* **2018**, *49*, 2766–2777. [CrossRef]
19. Gebauer, D.; Völkel, A.; Cölfen, H. Stable prenucleation calcium carbonate clusters. *Science* **2008**, *322*, 1819–1822. [CrossRef]
20. Turnbull, D.; Vonnegut, B. Nucleation catalysis. *Ind. Eng. Chem.* **1952**, *44*, 1292–1298. [CrossRef]
21. Wang, L.; Yang, L.; Zhang, D.; Xia, M.; Wang, Y.; Li, J.G. The role of lattice misfit on heterogeneous nucleation of pure aluminium. *Metall. Mater. Trans. A* **2016**, *47*, 5012–5022. [CrossRef]
22. Wang, L.; Lu, W.Q.; Hu, Q.D.; Xia, M.X.; Wang, Y.; Li, J.G. Interfacial tuning for the nucleation of liquid AlCu alloy. *Acta Mater.* **2017**, *139*, 75–85. [CrossRef]
23. Tóth, G.I.; Tegze, G.; Pusztai, T.; Gránásy, L. Heterogeneous crystal nucleation: The effect of lattice mismatch. *Phys. Rev. Lett.* **2012**, *108*, 025502. [CrossRef]
24. Fan, Z.; Men, H. A molecular dynamics study of heterogeneous nucleation in generic liquid/substrate systems with positive lattice misfit. *Mater. Res. Express* **2020**, *7*, 126501. [CrossRef]
25. Jiang, B.; Men, H.; Fan, Z. Atomic ordering in the liquid adjacent to an atomically rough solid surface. *Comput. Mater. Sci.* **2018**, *153*, 73–81. [CrossRef]
26. Fang, C.M.; Men, H.; Fan, Z. Effect of substrate chemistry on prenucleation. *Metall. Mater. Trans. A* **2018**, *49*, 6231–6242. [CrossRef]
27. Men, H.; Fan, Z. Heterogeneous nucleation mechanisms in systems with large lattice misfit demonstrated by the Pb(l)/Cu(s) system. *Metals* **2022**, *12*, 1583. [CrossRef]
28. Henderson, D.; Abraham, F.F.; Barker, J.A. The Ornstein-Zernike equation for a fluid in contact with a surface. *Mol. Phys.* **1976**, *31*, 1291. [CrossRef]
29. Abrahama, F.F.; Singh, Y. The structure of a hard-sphere fluid in contact with a soft repulsive wall. *J. Chem. Phys.* **1977**, *67*, 2384–2385. [CrossRef]
30. Abraham, F.F.; Singh, Y. Comment on "The structure of a hard sphere fluid in contact with a soft repulsive wall". *J. Chem. Phys.* **1978**, *68*, 4767–4768. [CrossRef]
31. Donnelly, S.E.; Birtcher, R.C.; Allen, C.W.; Morrison, I.; Furuya, K.; Song, M.H.; Mitsuishi, K.; Dahmen, U. Ordering in a fluid inert gas confined by flat surfaces. *Science* **2002**, *296*, 507–510. [CrossRef]
32. Fischer, J.; Methfessel, M. Born-Green-Yvon approach to the local densities of a fluid at interfaces. *Phys. Rev. A* **1980**, *22*, 2836–2843. [CrossRef]
33. Rull, L.F.; Toxvaerd, S. The structure and thermodynamics of a solid–fluid interface. *J. Chem. Phys.* **1983**, *78*, 3273–3278. [CrossRef]
34. Kyrlidis, A.; Brown, R.A. Density functional theory and atomistic simulation of the hard-sphere melt-solid interface. *Phys. Rev. E* **1995**, *51*, 5832–5845. [CrossRef] [PubMed]
35. Geysermans, P.; Gorse, D.; Pontikis, V. Molecular dynamics study of the solid-liquid interface. *J. Chem. Phys.* **2000**, *113*, 6382–6389. [CrossRef]
36. Magnussen, O.M.; Ocko, B.M.; Regan, M.J.; Penanen, K.; Pershan, P.S.; Deutsch, M. X-ray reflectivity measurements of surface layering in liquid mercury. *Phys. Rev. Lett.* **1995**, *74*, 4444–4447. [CrossRef] [PubMed]
37. Regan, M.J.; Kawamoto, E.H.; Lee, S.; Pershan, P.S.; Maskil, N.; Deutsch, M.; Magnussen, O.M.; Ocko, B.M.; Berman, L.E. Surface layering in liquid gallium: An X-Ray reflectivity study. *Phys. Rev. Lett.* **1995**, *75*, 2498–2501. [CrossRef] [PubMed]
38. Shpyrko, O.G.; Grigoriev, A.Y.; Steimer, C.; Pershan, P.S.; Lin, B.; Meron, M.; Graber, T.; Gerbhardt, J.; Ocko, B.; Deutsch, M. Anomalous layering at the liquid Sn surface. *Phys. Rev. B* **2004**, *70*, 224206. [CrossRef]
39. Huisman, W.J.; Peters, J.F.; Zwanenburg, M.J.; de Vries, S.A.; Derry, T.E.; Abernathy, D.; van der Veen, J.F. Layering of a liquid metal in contact with a hard wall. *Nature* **1997**, *390*, 379–381. [CrossRef]

40. Yu, C.J.; Richter, A.G.; Datta, A.; Durbin, M.K.; Dutta, P. Observation of molecular layering in thin liquid films using X-ray reflectivity. *Phys. Rev. Lett.* **1999**, *82*, 2326–2329. [CrossRef]

41. Reichert, H.; Klein, O.; Dosch, H.; Denk, M.; Honkimäki, V.; Lippmann, T.; Reiter, G. Observation of five-fold local symmetry in liquid lead. *Nature* **2000**, *408*, 839–841. [CrossRef]

42. Doerr, A.K.; Tolan, M.; Schlomka, J.P.; Press, W. Evidence for density anomalies of liquids at the solid/liquid interface. *Euro. Phys. Lett.* **2000**, *52*, 330–336. [CrossRef]

43. Grey, F.; Feidenhans'l, R.; Pedersen, J.S.; Nielsen, M.; Johnson, R.L. Pb/Ge(111) 1 × 1: An anisotropic two-dimensional liquid. *Phys. Rev. B* **1990**, *41*, 9519–9522. [CrossRef]

44. Huisman, W.J.; Peters, J.F.; Derks, J.W.; Ficke, H.G.; Abernathy, D.L.; van der Veen, J.F. A new X-ray diffraction method for structural investigations of solid-liquid interfaces. *Rev. Sci. Instrum.* **1997**, *68*, 4169–4176. [CrossRef]

45. Huisman, W.J.; van der Veen, J.F. Modelling the atomic density across a solid-liquid interface. *Surf. Sci.* **1998**, *404*, 866–870. [CrossRef]

46. Reedijk, M.F.; Arsic, J.; Theije, F.K.d.; McBride, M.T.; Peters, K.F.; Vlieg, E. Structure of liquid Sn on Ge(111). *Phys. Rev. B* **2001**, *64*, 033403. [CrossRef]

47. Reedijk, M.F.; Arsic, J.; Hollander, F.F.A.; de Vries, S.A.; Vlieg, E. Liquid order at the interface of KDP crystals with water: Evidence for icelike layers. *Phys. Rev. Lett.* **2003**, *90*, 066103. [CrossRef]

48. Schülli, T.U.; Daudin, R.; Renaud, G.; Vaysset, A.; Geaymond, O.; Pasturel, A. Substrate-enhanced supercooling in AuSi eutectic droplets. *Nature* **2010**, *464*, 1174–1177. [CrossRef]

49. Hohenberg, P.; Kohn, W. Inhomogeneous electron gas. *Phys. Rev.* **1964**, *136*, B864–B871. [CrossRef]

50. Kohn, W.; Sham, L.J. Self-consistent equations including exchange and correlation effects. *Phys. Rev.* **1965**, *140*, A1133–A1138. [CrossRef]

51. McMullen, W.E.; Oxtoby, D.W. A density functional approach to freezing transitions in molecular fluids: Dipolar hard spheres. *J. Chem. Phys.* **1987**, *86*, 4146–4156. [CrossRef]

52. Curtin, W.A. Density-functional theory of the solid-liquid interface. *Phys. Rev. Lett.* **1987**, *59*, 1228–1231. [CrossRef]

53. Sikkenk, J.H.; Indekeu, J.O.; van Leeuwen, J.M.J.; Vossnack, E.O. Molecular-dynamics simulation of wetting and drying at solid-fluid interfaces. *Phys. Rev. Lett.* **1987**, *59*, 98–101. [CrossRef]

54. Ma, W.-J.; Banavar, J.R.; Koplik, J. A molecular dynamics study of freezing in a confined geometry. *J. Chem. Phys.* **1992**, *97*, 485–493. [CrossRef]

55. Hook, J.R.; Hall, H.E. *Solid State Physics*, 2nd ed.; Wiley: Chichester, UK, 1991.

56. Steinhardt, P.J.; Nelson, D.R.; Ronchetti, M. Bond-orientational order in liquids and glasses. *Phys. Rev. B* **1983**, *28*, 784–805. [CrossRef]

57. Ten Wolde, P.R.; Ruiz-Montero, M.J.; Frenkel, D. Numerical evidence for bcc ordering at the surface of a critical fcc nucleus. *Phys. Rev. Lett.* **1995**, *75*, 2714–2717. [CrossRef]

58. Auer, S.; Frenkel, D. Numerical prediction of absolute crystallization rates in hard-sphere colloids. *J. Chem. Phys.* **2004**, *120*, 3015–3029. [CrossRef]

59. Auer, S.; Frenkel, D. Prediction of absolute crystal-nucleation rate in hard-sphere colloids. *Nature* **2001**, *409*, 1020–1023. [CrossRef]

60. Zope, R.R.; Mishin, Y. Interatomic potentials for atomistic simulations of the Ti-Al system. *Phys. Rev. B* **2003**, *68*, 024102. [CrossRef]

61. Hoyt, J.J.; Garvin, J.W.; Webb III, E.B.; Asta, M. An embedded atom method interatomic potential for the Cu-Pb system. *Model. Simul. Mater. Sci. Eng.* **2003**, *11*, 287–299. [CrossRef]

62. Plimpton, S. Fast parallel algorithms for short-range molecular dynamics. *J. Comput. Phys.* **1995**, *117*, 1–19. [CrossRef]

63. Grimmer, H.; Bollmann, W.; Warrington, D.H. Coincidence-site lattices and complete pattern-shift in cubic crystals. *Acta Crystallogr. A* **1974**, *30*, 197–207. [CrossRef]

64. Men, H.; Fan, Z. Molecular dynamics simulations on effect of surface roughness of amorphous substrate on nucleation in liquid Al. *Metals* **2022**, *12*, 1529. [CrossRef]

65. Blöchl, P.E. Projector augmented-wave method. *Phys. Rev. B* **1994**, *50*, 17953–17979. [CrossRef] [PubMed]

66. Kresse, G.; Joubert, J. From ultrasoft pseudopotentials to the projector augmented-wave method. *Phys. Rev. B* **1999**, *59*, 1758–1775. [CrossRef]

67. Perdew, J.P.; Burke, K.; Ernzerhof, M. Generalized gradient approximation made simple. *Phys. Rev. Lett.* **1996**, *77*, 3865–3868. [CrossRef]

68. Rosato, V.; Guillope, M.; Legrand, B. Thermodynamical and structural properties of f.c.c. transition metals using a simple tight-binding model. *Philos. Mag. A* **1989**, *59*, 321–336. [CrossRef]

69. Wang, S.H.; Wang, Y.; Ramasse., Q.; Fan, Z. The nature of native MgO in Mg and its alloys. *Metal. Mater. Trans. A* **2020**, *51*, 2957–2974. [CrossRef]

70. Li, H.-T.; Wang, Y.; Fan, Z. Mechanisms of enhanced heterogeneous nucleation during solidification in binary Al-Mg alloys. *Acta Mater.* **2012**, *60*, 1528–1537. [CrossRef]

71. Wang, Y.; Fan, Z.; Zhou, X.; Thompson, G.E. Characterisation of magnesium oxide and its interface with α-Mg in Mg-Al-based alloys. *Phil. Mag. Lett.* **2011**, *91*, 516–529. [CrossRef]

72. Wang, Y.; Li, H.-T.; Fan, Z. Oxidation of aluminium alloy melts and inoculation by oxide particles. *Trans. Indian Inst. Met.* **2021**, *65*, 653–661. [CrossRef]

73.   Kim, K. Formation of endogenous MgO and MgAl$_2$O$_4$ particles and their possibility of acting as substrate for heterogeneous nucleation of aluminum grains. *Surf. Interface Anal.* **2015**, *47*, 429–438. [CrossRef]
74.   Fang, C.M.; Fan, Z. Prenucleation at the interface between MgO and liquid magnesium: An ab initio molecular dynamics study. *Metal. Mater. Trans. A* **2020**, *51*, 788–797. [CrossRef]
75.   Fang, C.M.; Fan, Z. Prenucleation at the liquid-Al/α-Al$_2$O$_3$ and the liquid-Al/MgO interfaces. *Comp. Mater. Sci.* **2020**, *171*, 109258. [CrossRef]
76.   Fang, C.M.; Fan, Z. Atomic ordering at the interfaces between liquid Al and MgO: An ab initio molecular dynamics study. *Philos. Mag. Lett.* **2020**, *100*, 235–244. [CrossRef]
77.   Fang, C.M.; Yasmin, S.; Fan, Z. Interfacial interaction and prenucleation at liquid-Al/γ-Al$_2$O$_3$\{1 1 1\} interfaces from ab initio molecular dynamics simulations. *J. Phys. Commun.* **2021**, *5*, 015007. [CrossRef]
78.   Fang, C.M.; Fan, Z. Atomic ordering at the Liquid-Al/MgAl$_2$O$_4$\{111\} Interfaces: Ab initio molecular dynamics simulations. *Metal. Mater. Trans. A* **2020**, *51*, 6318–6326. [CrossRef]
79.   Verwey, E.J.W. The crystal structure of γ-Fe$_2$O$_3$ and γ-Al$_2$O$_3$. *J. Z. Krist.* **1935**, *91*, 65–69. [CrossRef]
80.   Gibbs, J. *The Collected Works of J. Willard Gibbs*; Langman, Green and Co.: New York, NY, USA, 1928; Volume 1.
81.   Men, H.; Fan, Z. An analytical model for solute segregation at liquid metal/solid substrate interface. *Metall. Mater. Trans. A* **2014**, *45*, 5508–5516. [CrossRef]
82.   Fan, Z.; Wang, Y.; Zhang, Y.; Qin, T.; Zhou, X.R.; Thompson, G.E.; Pennycook, T.; Hashimoto, T. Grain refining mechanism in the Al/Al–Ti–B system. *Acta Mater.* **2015**, *84*, 292–304. [CrossRef]
83.   Wang, Y.; Fang, C.M.; Zhou, L.; Hashimoto, T.; Zhou, X.; Ramasse, Q.M.; Fan, Z. Mechanism for Zr poisoning of Al-Ti-B based grain refiners. *Acta Mater.* **2019**, *164*, 428–439. [CrossRef]
84.   Jones, G.P.; Pearson, J. Factors affecting the grain-refinement of aluminium using titanium and boron additives. *Metall. Trans. B* **1976**, *7*, 223–234. [CrossRef]
85.   Jones, G.P. *Solidification Processing 1987*; The Institute of Metals: London, UK, 1988; p. 496.
86.   Greer, A.L.; Bunn, A.M.; Tronche, A.; Evans, P.V.; Bristow, D.J. Modelling of inoculation of metallic melts: Application to grain refinement of aluminium by Al-Ti-B. *Acta Mater.* **2000**, *48*, 2823–2835. [CrossRef]
87.   Quested, T.E.; Greer, A.L. The effect of the size distribution of inoculant particles on as-cast grain size in aluminium alloys. *Acta Mater.* **2004**, *52*, 3859–3868. [CrossRef]
88.   Kelton, K.F.; Greer, A.L.; Herlach, D.M.; Holland-Moritz, D. The influence of order on the nucleation barrier. *MRS Bull.* **2004**, *29*, 940–944. [CrossRef]
89.   Fan, Z.; Men, H. An overview on atomistic mechanisms of heterogeneous nucleation. *Metals* **2022**, *12*, 1547. [CrossRef]
90.   Fan, Z.; Men, H. Heterogeneous nucleation and grain initiation on a single substrate. *Metals* **2022**, *12*, 1454. [CrossRef]
91.   Fan, Z.; Men, H.; Wang, Y.; Que, Z.P. A new atomistic mechanism for heterogeneous nucleation in the systems with negative lattice misfit: Creating a 2D template for crystal growth. *Metals* **2021**, *11*, 478. [CrossRef]